Non-associated flow rule with symmetric stiffness modulus for isotropic-kinematic hardening and its application for earing in circular cup drawing

Taejoon Park, Kwansoo Chung *

Department of Materials Science and Engineering, Research Institute of Advanced Materials, Engineering Research Institute, Seoul National University, Building 30, Room 413, 1 Gwanak-ro, Gwanak-gu, Seoul 151-744, Republic of Korea

ARTICLE INFO

ABSTRACT

Under a standard derivation, the stiffness modulus for the non-associated flow rule is asymmetric since its plastic potential (for the plastic strain increment under the normality rule) differs from the plastic yield stress function (to define the elastic range). A new formulation was developed in this work, which leads to the symmetric stiffness modulus for the non-associated flow rule, under the framework of the combined isotropic-kinematic hardening law for generalization purposes. As for its application, the non-quadratic Yld2000-2d (Barlat et al., 2003) function (and Hill's (1948) function for comparison) was utilized to validate the formulation for earing in circular cup drawing of AA2090-T3 and AA5042 sheets, which successfully represented 6 and 8 ears, respectively.

© 2012 Elsevier Ltd. All rights reserved.

1. Introduction

For the optimization of sheet forming processes utilizing computational methods, the constitutive model which can properly account for forming related phenomena such as failure and springback as well as wrinkling is required. Therefore, to ensure the capability to predict such phenomena, various material models have been developed for isotropic and anisotropic sheets to describe their plastic behavior such as the plastic strain increment, yielding and hardening behavior. In this effort, the most common practice has been to formulate the plastic deformation based on the normality rule, in which the (anisotropic) plastic strain increment is normal to the (anisotropic) yield surface (therefore, the plastic potential to define the plastic strain increment by the normality rule is identical with the plastic stress function to define the yield surface or the elastic stress field): the associated flow rule. Besides its intrinsic simplicity, the associated flow rule amply satisfies Drucker's (1959) stability postulate regarding the dissipative nature of the plastic work defined for a class of stable materials.

In order to account for planar anisotropy (of sheets), various yield functions have been developed. Hill (1948) proposed one of the most popular quadratic yield functions, while Hill (1979), Barlat et al. (1991, 1997, 2003, 2005), Banabic et al. (2005) and Cazacu et al. (2006) developed non-quadratic yield functions. Besides, Hill (1987), Barlat and Chung (1993), Barlat et al. (1993), Kim et al. (2007) described planar anisotropy based on plastic strain rate potentials. Under the framework of the associated flow rule, each of these plastic yield stress functions (or plastic strain rate poten-

tials) is supposed to simultaneously represent all measured anisotropic quantities such as yield stresses and R-values (width-to-thickness strain ratio), which is not always so successful since plastic yield functions (or plastic strain rate potentials) have a limited number of anisotropic coefficients to account for all the measured anisotropic quantities, especially for sheets whose anisotropy is so strong.

A non-associated flow rule is an alternative way to effectively represent anisotropy utilizing a plastic yield stress function (or a plastic strain rate potential) having a limited number of anisotropic coefficients. In the non-associated flow rule, the plastic potential (to derive the anisotropic plastic strain increment by the normality rule) is different from the plastic yield stress function (to describe anisotropic yield stresses) in principle, unlike the associated flow rule. Since two separate sets of anisotropic coefficients can be assigned for each of the plastic potential and the plastic stress function, respectively, the required number of the anisotropic coefficients for each plastic stress function or plastic potential to describe measured anisotropic quantities reduces to half for the non-associated flow rule, compared to the associated flow rule (Lademo et al., 1999). Stoughton (2002), Taherizadeh et al. (2010) and Mohr et al. (2010) proposed a non-associated model based on Hill's (1948) quadratic function, while Cvitanic et al. (2008), Taherizadeh et al. (2011) considered the Karafillis and Boyce (1993) non-quadratic function as well as Hill's (1948) function. In addition, experiments by Spitzig et al. (1975) reported that the associated flow rule was violated during the plastic deformation under hydrostatic pressure so that Brunig (1999), Brunig et al. (2000), Stoughton and Yoon (2004) proposed non-associated flow models based on pressure sensitive yield criteria. As for the issue of stability, Stoughton and Yoon (2006, 2008) derived and discussed general constraints on a non-associated flow model

---

* Corresponding author.
  E-mail address: kchung@snu.ac.kr (K. Chung).

required to guarantee uniqueness and positive plastic work, as well as to avoid yield point elongation in proportional loading.

The most common practice to evaluate the anisotropy of sheets is to experimentally measure earing in circular cup drawing, which is also an important operation to form a cylindrical cup (for such as beverage can applications). The non-associated flow model in which Hill's (1948) function, or similar functions with at most four anisotropic coefficients (for sheet forming processes) was used for both the plastic potential and the yield function has been so effective and popular to simulate anisotropy which would require at most eight anisotropic coefficients for a single anisotropic function that was based on the associated flow rule. For such a case, at most four ears develop in cylindrical cup drawing.

However, if the anisotropy of sheets requires more than eight anisotropic coefficients for the associated flow rule (which signifies that more than four ears develop in cylindrical cup drawing), sophisticated plastic functions having more than four anisotropic coefficients are necessary for the application of the non-associated flow rule. Therefore, a non-associated flow rule was developed in this work utilizing the Yld2000-2d (Barlat et al., 2003) anisotropic yield function having eight anisotropic coefficients, in particular for AA2090-T3 and AA5042 sheets, which developed six or eight ears in cylindrical cup drawing (refer to the NUMISHEET benchmark for earing of AA5042 sheets proposed by Yoon and Dick (2011)). If the associated flow rule were applied for these cases, plastic yield functions such as Yld2004–18p (Barlat et al., 2005) or CPB06ex2 (Cazacu et al., 2006) having 12 to 18 coefficients would have been required to simulate six or eight ears (Yoon et al., 2000, 2004, 2010; Soare and Barlat, 2011).

Under a standard derivation, the stiffness modulus for the non-associated flow rule is asymmetric since its plastic potential (for the plastic strain increment under the normality rule) differs from the plastic yield stress function (to define the elastic range). Note that a new formulation was also developed in this work, which lead to a symmetric stiffness modulus for the non-associated flow rule, under the framework of the Chaboche (1986, 1991) type isotropic-kinematic hardening model (Chung et al., 2005) for generalization purposes. The symmetric stiffness modulus provides a basis of much more effective numerical formulations compared to the asymmetric stiffness modulus.

2. Non-associated flow rule

2.1. Flow formulation for asymmetric and symmetric stiffness moduli

In the non-associated flow rule, the yield criterion to define anisotropic yield stresses (or elastic range) is described by

$$f(\boldsymbol{\sigma} - \boldsymbol{\alpha}) - \bar{\sigma}_{iso}(\bar{\varepsilon}) = 0, \tag{1}$$

where $f(\boldsymbol{\sigma} - \boldsymbol{\alpha})$ is the yield stress function (to define the yield surface), $\boldsymbol{\sigma}$ is the Cauchy stress and $\boldsymbol{\alpha}$ is the back-stress for the kinematic hardening, while the effective stress (related to the isotropic hardening), $\bar{\sigma}_{iso}$, is the size of the yield surface as a function of the accumulative effective strain, $\bar{\varepsilon}(\equiv \int d\bar{\varepsilon})$. As for the anisotropic plastic strain increment, the normality flow rule is

$$d\boldsymbol{\varepsilon}^p = d\bar{\varepsilon}_p \frac{\partial g}{\partial(\boldsymbol{\sigma} - \boldsymbol{\alpha})}, \tag{2}$$

where $g(\boldsymbol{\sigma} - \boldsymbol{\alpha})$ and $d\bar{\varepsilon}_p$ are the plastic potential and its conjugate effective quantity defined by the following plastic work equivalence principle (Chung et al., 2005), respectively; i.e.,

$$dw_{iso} = (\boldsymbol{\sigma} - \boldsymbol{\alpha}) : d\boldsymbol{\varepsilon}^p = \bar{\sigma}_{iso}d\bar{\varepsilon} = \bar{\sigma}_{pot}d\bar{\varepsilon}_p. \tag{3}$$

Here, $\bar{\sigma}_{pot}$ is the effective quantity to describe the size of the plastic potential, which is defined by the following potential criterion as similarly done for the effective stress in the yield criterion; i.e.,

$$g(\boldsymbol{\sigma} - \boldsymbol{\alpha}) - \bar{\sigma}_{pot}(\bar{\varepsilon}_p) = 0. \tag{4}$$

with $\bar{\varepsilon}_p(\equiv \int d\bar{\varepsilon}_p)$. Therefore,

$$\frac{d\bar{\varepsilon}}{d\bar{\varepsilon}_p} = \frac{\bar{\sigma}_{pot}}{\bar{\sigma}_{iso}} = \frac{g(\boldsymbol{\sigma} - \boldsymbol{\alpha})}{f(\boldsymbol{\sigma} - \boldsymbol{\alpha})}. \tag{5}$$

Note that f and g are first order homogeneous functions sharing the same back-stress (as their centers) as schematically shown in Fig. 1(a), in which the reference value to define their sizes is $\sigma_1 - \alpha_1$ (as an example in the 2-D space). Fig. 1(a) illustrates that, when a yield stress surface f is defined with its size, $\bar{\sigma}_{iso}$, the ratio between the effective quantities defined in Eq. (5) varies according to $\bar{\sigma}_{iso}d\bar{\varepsilon} = \bar{\sigma}_{pot/A}d\bar{\varepsilon}_{p/A} = \bar{\sigma}_{pot/B}d\bar{\varepsilon}_{p/B}$ where A and B represent different stress states on the yield stress surface f. Therefore, when the isotropic hardening (the expansion of the yield stress surface during plastic deformation) is expressed by $\bar{\sigma}_{iso}(\bar{\varepsilon})$, equivalent hardening expressions are also obtained for each stress state as $\bar{\sigma}_{pot/A}(\bar{\varepsilon}_{p/A})$ or $\bar{\sigma}_{pot/B}(\bar{\varepsilon}_{p/B})$ after considering the ratio obtained in Eq. (5), as schematically shown in Fig. 1(b).

The linear elastic constitutive law for the Jaumann (or co-rotational) stress rate of the Cauchy stress is

$$d\boldsymbol{\sigma} = \underset{\sim}{\boldsymbol{C}}^e \cdot d\boldsymbol{\varepsilon}^e = \underset{\sim}{\boldsymbol{C}}^e \cdot (d\boldsymbol{\varepsilon} - d\boldsymbol{\varepsilon}^p). \tag{6}$$

Here, $\boldsymbol{C}^e$, $d\boldsymbol{\varepsilon}^e$ and $d\boldsymbol{\varepsilon}^p$ are the elastic stiffness tensor, the elastic strain increment and the plastic strain increment, respectively. Considering Eqs. (2) and (6) becomes,

$$\begin{aligned} d\boldsymbol{\sigma} &= \underset{\sim}{\boldsymbol{C}}^e \cdot \left(d\boldsymbol{\varepsilon} - \frac{\partial g}{\partial(\boldsymbol{\sigma} - \boldsymbol{\alpha})} d\bar{\varepsilon}_p \right) \\ &= \underset{\sim}{\boldsymbol{C}}^e \cdot \left(d\boldsymbol{\varepsilon} - \frac{\partial g}{\partial(\boldsymbol{\sigma} - \boldsymbol{\alpha})} \frac{f(\boldsymbol{\sigma} - \boldsymbol{\alpha})}{g(\boldsymbol{\sigma} - \boldsymbol{\alpha})} d\bar{\varepsilon} \right). \end{aligned} \tag{7}$$

Then, the yield criterion described in Eq. (1) leads to, by the consistency condition,

$$\begin{aligned} &\frac{\partial f}{\partial(\boldsymbol{\sigma} - \boldsymbol{\alpha})} : d(\boldsymbol{\sigma} - \boldsymbol{\alpha}) - \frac{\partial \bar{\sigma}_{iso}}{\partial \bar{\varepsilon}} d\bar{\varepsilon} \\ &\quad = \frac{\partial f}{\partial(\boldsymbol{\sigma} - \boldsymbol{\alpha})} : \left[\underset{\sim}{\boldsymbol{C}}^e \cdot \left(d\boldsymbol{\varepsilon} - \frac{f(\boldsymbol{\sigma} - \boldsymbol{\alpha})}{g(\boldsymbol{\sigma} - \boldsymbol{\alpha})} d\bar{\varepsilon} \frac{\partial g}{\partial(\boldsymbol{\sigma} - \boldsymbol{\alpha})} \right) - \frac{\partial \boldsymbol{\alpha}}{\partial \bar{\varepsilon}} d\bar{\varepsilon} \right] \\ &\quad\quad - \frac{\partial \bar{\sigma}_{iso}}{\partial \bar{\varepsilon}} d\bar{\varepsilon} = 0. \end{aligned} \tag{8}$$

Note here that $\frac{\partial \boldsymbol{\alpha}}{\partial \bar{\varepsilon}}$ is defined by the hardening model to represent the translation of the yield surface. In this work, the back-stress increment of Chaboche (1986, 1991) type nonlinear kinematic hardening model (Chung et al., 2005) was utilized to define the back-stress evolution; i.e.,

$$\frac{\partial \boldsymbol{\alpha}}{\partial \bar{\varepsilon}} = h_2 \left(\frac{h_1}{h_2} \frac{(\boldsymbol{\sigma} - \boldsymbol{\alpha})}{\bar{\sigma}_{iso}(\boldsymbol{\sigma} - \boldsymbol{\alpha})} - \alpha \right) \tag{9}$$

where h_1 and h_2 are kinematic hardening parameters to define the rate of kinematic translation. As discussed by Chung et al. (2005), the back-stress evolution law described in Eq. (9) guarantees the same hardening as the full isotropic hardening under monotonous proportional loading condition since the translation rate of the yield surface is proportional to the initial (anisotropic) yield stresses, preserving the initial stress anisotropy.

After further manipulations from Eq. (8), the effective strain increment becomes,

$$d\bar{\varepsilon} = \frac{\frac{\partial f}{\partial(\boldsymbol{\sigma} - \boldsymbol{\alpha})} : \underset{\sim}{\boldsymbol{C}}^e \cdot d\boldsymbol{\varepsilon}}{\frac{f(\boldsymbol{\sigma} - \boldsymbol{\alpha})}{g(\boldsymbol{\sigma} - \boldsymbol{\alpha})} \frac{\partial f}{\partial(\boldsymbol{\sigma} - \boldsymbol{\alpha})} : \underset{\sim}{\boldsymbol{C}}^e \cdot \frac{\partial g}{\partial(\boldsymbol{\sigma} - \boldsymbol{\alpha})} + \frac{\partial f}{\partial(\boldsymbol{\sigma} - \boldsymbol{\alpha})} : \frac{\partial \boldsymbol{\alpha}}{\partial \bar{\varepsilon}} + \frac{\partial \bar{\sigma}_{iso}}{\partial \bar{\varepsilon}}} \tag{10}$$

or

$$d\bar{\varepsilon}_p = \frac{\frac{\partial f}{\partial(\boldsymbol{\sigma} - \boldsymbol{\alpha})} : \underset{\sim}{\boldsymbol{C}}^e \cdot d\boldsymbol{\varepsilon}}{\frac{\partial f}{\partial(\boldsymbol{\sigma} - \boldsymbol{\alpha})} : \underset{\sim}{\boldsymbol{C}}^e \cdot \frac{\partial g}{\partial(\boldsymbol{\sigma} - \boldsymbol{\alpha})} + \frac{\partial f}{\partial(\boldsymbol{\sigma} - \boldsymbol{\alpha})} : \frac{\partial \boldsymbol{\alpha}}{\partial \bar{\varepsilon}_p} + \frac{\partial \bar{\sigma}_{iso}}{\partial \bar{\varepsilon}_p}}. \tag{11}$$
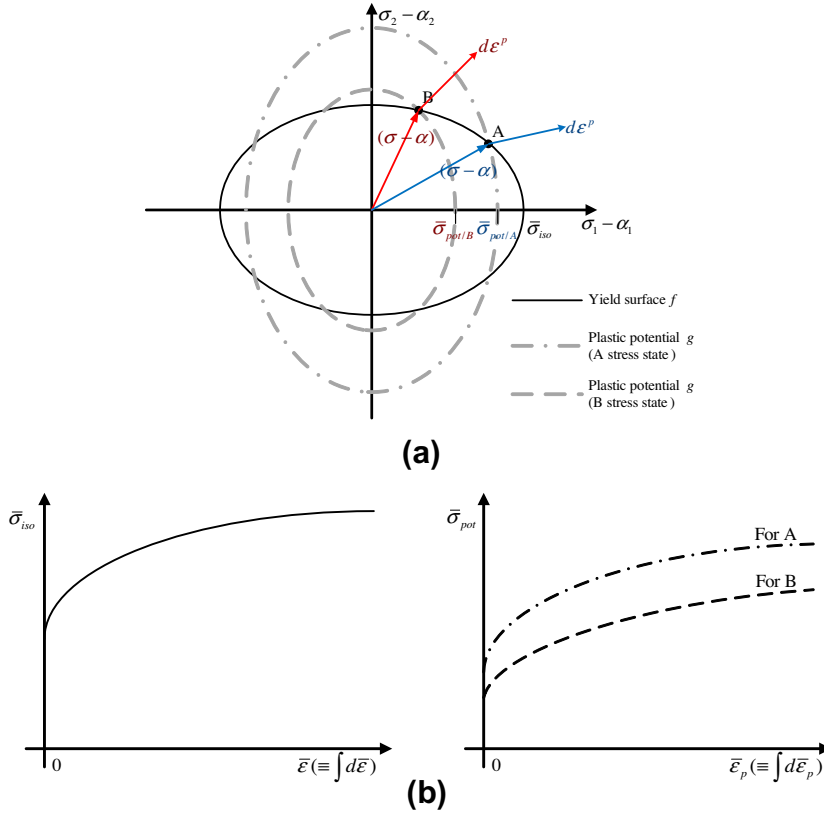
Fig. 1. Schematic views of (a) the yield stress and plastic potential surfaces and (b) the isotropic hardening (the expansion of the surfaces) defined for each surface considering the stress state.

Substituting Eq. (10) or Eq. (11) into Eq. (7), the following asymmetric elasto-plastic tangent (or stiffness) modulus is obtained

$$
\frac{d\boldsymbol{\sigma}}{d\boldsymbol{\varepsilon}} = \underset{\sim}{\boldsymbol{C}^e} - \frac{\frac{f(\boldsymbol{\sigma}-\boldsymbol{\alpha})}{g(\boldsymbol{\sigma}-\boldsymbol{\alpha})}\underset{\sim}{\boldsymbol{C}^e} : \frac{\partial g}{\partial(\boldsymbol{\sigma}-\boldsymbol{\alpha})} \otimes \frac{\partial f}{\partial(\boldsymbol{\sigma}-\boldsymbol{\alpha})} : \underset{\sim}{\boldsymbol{C}^e}}{\frac{f(\boldsymbol{\sigma}-\boldsymbol{\alpha})}{g(\boldsymbol{\sigma}-\boldsymbol{\alpha})}\frac{\partial f}{\partial(\boldsymbol{\sigma}-\boldsymbol{\alpha})} : \underset{\sim}{\boldsymbol{C}^e} \cdot \frac{\partial g}{\partial(\boldsymbol{\sigma}-\boldsymbol{\alpha})} + \frac{\partial f}{\partial(\boldsymbol{\sigma}-\boldsymbol{\alpha})} : \frac{\partial \boldsymbol{\alpha}}{\partial \bar{\varepsilon}} + \frac{\partial \bar{\sigma}_{iso}}{\partial \bar{\varepsilon}}}
\tag{12}
$$

or

$$
\frac{d\boldsymbol{\sigma}}{d\boldsymbol{\varepsilon}} = \underset{\sim}{\boldsymbol{C}^e} - \frac{\underset{\sim}{\boldsymbol{C}^e} : \frac{\partial g}{\partial(\boldsymbol{\sigma}-\boldsymbol{\alpha})} \otimes \frac{\partial f}{\partial(\boldsymbol{\sigma}-\boldsymbol{\alpha})} : \underset{\sim}{\boldsymbol{C}^e}}{\frac{\partial f}{\partial(\boldsymbol{\sigma}-\boldsymbol{\alpha})} : \underset{\sim}{\boldsymbol{C}^e} \cdot \frac{\partial g}{\partial(\boldsymbol{\sigma}-\boldsymbol{\alpha})} + \frac{\partial f}{\partial(\boldsymbol{\sigma}-\boldsymbol{\alpha})} : \frac{\partial \boldsymbol{\alpha}}{\partial \bar{\varepsilon}_p} + \frac{\partial \bar{\sigma}_{iso}}{\partial \bar{\varepsilon}_p}}.
\tag{13}
$$

Since the asymmetric stiffness modulus is cumbersome for numerical formulations, a symmetric stiffness modulus is derived here considering the consistency condition applied for the plastic potential defined in Eq. (4); i.e.,

$$
\frac{\partial g}{\partial(\boldsymbol{\sigma}-\boldsymbol{\alpha})} : d(\boldsymbol{\sigma}-\boldsymbol{\alpha}) - \frac{\partial \bar{\sigma}_{pot}}{\partial \bar{\varepsilon}_p} d\bar{\varepsilon}_p = \frac{\partial g}{\partial(\boldsymbol{\sigma}-\boldsymbol{\alpha})}
$$
$$
: \left[\underset{\sim}{\boldsymbol{C}^e} \cdot \left(d\boldsymbol{\varepsilon} - \frac{f(\boldsymbol{\sigma}-\boldsymbol{\alpha})}{g(\boldsymbol{\sigma}-\boldsymbol{\alpha})} d\bar{\varepsilon} \frac{\partial g}{\partial(\boldsymbol{\sigma}-\boldsymbol{\alpha})} \right) - \frac{\partial \boldsymbol{\alpha}}{\partial \bar{\varepsilon}} d\bar{\varepsilon} \right] - \frac{\partial \bar{\sigma}_{pot}}{\partial \bar{\varepsilon}} d\bar{\varepsilon} = 0. \tag{14}
$$

Therefore,

$$
d\bar{\varepsilon} = \frac{\frac{\partial g}{\partial(\boldsymbol{\sigma}-\boldsymbol{\alpha})} : \underset{\sim}{\boldsymbol{C}^e} \cdot d\boldsymbol{\varepsilon}}{\frac{f(\boldsymbol{\sigma}-\boldsymbol{\alpha})}{g(\boldsymbol{\sigma}-\boldsymbol{\alpha})} \frac{\partial g}{\partial(\boldsymbol{\sigma}-\boldsymbol{\alpha})} : \underset{\sim}{\boldsymbol{C}^e} \cdot \frac{\partial g}{\partial(\boldsymbol{\sigma}-\boldsymbol{\alpha})} + \frac{\partial g}{\partial(\boldsymbol{\sigma}-\boldsymbol{\alpha})} : \frac{\partial \boldsymbol{\alpha}}{\partial \bar{\varepsilon}} + \frac{\partial \bar{\sigma}_{pot}}{\partial \bar{\varepsilon}}}
\tag{15}
$$

and

$$
d\bar{\varepsilon}_p = \frac{\frac{\partial g}{\partial(\boldsymbol{\sigma}-\boldsymbol{\alpha})} : \underset{\sim}{\boldsymbol{C}^e} \cdot d\boldsymbol{\varepsilon}}{\frac{\partial g}{\partial(\boldsymbol{\sigma}-\boldsymbol{\alpha})} : \underset{\sim}{\boldsymbol{C}^e} \cdot \frac{\partial g}{\partial(\boldsymbol{\sigma}-\boldsymbol{\alpha})} + \frac{\partial g}{\partial(\boldsymbol{\sigma}-\boldsymbol{\alpha})} : \frac{\partial \boldsymbol{\alpha}}{\partial \bar{\varepsilon}_p} + \frac{\partial \bar{\sigma}_{pot}}{\partial \bar{\varepsilon}_p}}.
\tag{16}
$$

Substituting Eq. (15) or Eq. (16) into Eq. (7), the following symmetric stiffness modulus is obtained:

$$
\frac{d\boldsymbol{\sigma}}{d\boldsymbol{\varepsilon}} = \underset{\sim}{\boldsymbol{C}^e} - \frac{\frac{f(\boldsymbol{\sigma}-\boldsymbol{\alpha})}{g(\boldsymbol{\sigma}-\boldsymbol{\alpha})}\underset{\sim}{\boldsymbol{C}^e} : \frac{\partial g}{\partial(\boldsymbol{\sigma}-\boldsymbol{\alpha})} \otimes \frac{\partial g}{\partial(\boldsymbol{\sigma}-\boldsymbol{\alpha})} : \underset{\sim}{\boldsymbol{C}^e}}{\frac{f(\boldsymbol{\sigma}-\boldsymbol{\alpha})}{g(\boldsymbol{\sigma}-\boldsymbol{\alpha})}\frac{\partial g}{\partial(\boldsymbol{\sigma}-\boldsymbol{\alpha})} : \underset{\sim}{\boldsymbol{C}^e} \cdot \frac{\partial g}{\partial(\boldsymbol{\sigma}-\boldsymbol{\alpha})} + \frac{\partial g}{\partial(\boldsymbol{\sigma}-\boldsymbol{\alpha})} : \frac{\partial \boldsymbol{\alpha}}{\partial \bar{\varepsilon}} + \frac{\partial \bar{\sigma}_{pot}}{\partial \bar{\varepsilon}}},
\tag{17}
$$

or

$$
\frac{d\boldsymbol{\sigma}}{d\boldsymbol{\varepsilon}} = \underset{\sim}{\boldsymbol{C}^e} - \frac{\underset{\sim}{\boldsymbol{C}^e} : \frac{\partial g}{\partial(\boldsymbol{\sigma}-\boldsymbol{\alpha})} \otimes \frac{\partial g}{\partial(\boldsymbol{\sigma}-\boldsymbol{\alpha})} : \underset{\sim}{\boldsymbol{C}^e}}{\frac{\partial g}{\partial(\boldsymbol{\sigma}-\boldsymbol{\alpha})} : \underset{\sim}{\boldsymbol{C}^e} \cdot \frac{\partial g}{\partial(\boldsymbol{\sigma}-\boldsymbol{\alpha})} + \frac{\partial g}{\partial(\boldsymbol{\sigma}-\boldsymbol{\alpha})} : \frac{\partial \boldsymbol{\alpha}}{\partial \bar{\varepsilon}_p} + \frac{\partial \bar{\sigma}_{pot}}{\partial \bar{\varepsilon}_p}}.
\tag{18}
$$

Here, after considering Eqs. (10) and (15), the derivatives of the plastic potential size, $\frac{\partial \bar{\sigma}_{pot}}{\partial \bar{\varepsilon}}$ and $\frac{\partial \bar{\sigma}_{pot}}{\partial \bar{\varepsilon}_p}$, are dependent on the strain increment, $d\boldsymbol{\varepsilon}$:

$$
\frac{\partial \bar{\sigma}_{pot}}{\partial \bar{\varepsilon}} = \frac{\frac{\partial g}{\partial(\boldsymbol{\sigma}-\boldsymbol{\alpha})} : \underset{\sim}{\boldsymbol{C}^e} \cdot d\boldsymbol{\varepsilon}}{\frac{\partial f}{\partial(\boldsymbol{\sigma}-\boldsymbol{\alpha})} : \underset{\sim}{\boldsymbol{C}^e} \cdot d\boldsymbol{\varepsilon}} \left(\frac{f(\boldsymbol{\sigma}-\boldsymbol{\alpha})}{g(\boldsymbol{\sigma}-\boldsymbol{\alpha})} \frac{\partial f}{\partial(\boldsymbol{\sigma}-\boldsymbol{\alpha})} : \underset{\sim}{\boldsymbol{C}^e} \cdot \frac{\partial g}{\partial(\boldsymbol{\sigma}-\boldsymbol{\alpha})} + \frac{\partial f}{\partial(\boldsymbol{\sigma}-\boldsymbol{\alpha})} \right.
$$
$$
\left. : \frac{\partial \boldsymbol{\alpha}}{\partial \bar{\varepsilon}} + \frac{\partial \bar{\sigma}_{iso}}{\partial \bar{\varepsilon}} \right) - \frac{f(\boldsymbol{\sigma}-\boldsymbol{\alpha})}{g(\boldsymbol{\sigma}-\boldsymbol{\alpha})} \frac{\partial g}{\partial(\boldsymbol{\sigma}-\boldsymbol{\alpha})} : \underset{\sim}{\boldsymbol{C}^e} \cdot \frac{\partial g}{\partial(\boldsymbol{\sigma}-\boldsymbol{\alpha})} + \frac{\partial g}{\partial(\boldsymbol{\sigma}-\boldsymbol{\alpha})} : \frac{\partial \boldsymbol{\alpha}}{\partial \bar{\varepsilon}}. \tag{19}
$$

and

$$
\frac{\partial \bar{\sigma}_{pot}}{\partial \bar{\varepsilon}_p} = \frac{\frac{\partial g}{\partial(\boldsymbol{\sigma}-\boldsymbol{\alpha})} : \underset{\sim}{\boldsymbol{C}^e} \cdot d\boldsymbol{\varepsilon}}{\frac{\partial f}{\partial(\boldsymbol{\sigma}-\boldsymbol{\alpha})} : \underset{\sim}{\boldsymbol{C}^e} \cdot d\boldsymbol{\varepsilon}} \left(\frac{\partial f}{\partial(\boldsymbol{\sigma}-\boldsymbol{\alpha})} : \underset{\sim}{\boldsymbol{C}^e} \cdot \frac{\partial g}{\partial(\boldsymbol{\sigma}-\boldsymbol{\alpha})} + \frac{\partial f}{\partial(\boldsymbol{\sigma}-\boldsymbol{\alpha})} : \frac{\partial \boldsymbol{\alpha}}{\partial \bar{\varepsilon}_p} + \frac{\partial \bar{\sigma}_{iso}}{\partial \bar{\varepsilon}_p} \right)
$$
$$
- \frac{\partial g}{\partial(\boldsymbol{\sigma}-\boldsymbol{\alpha})} : \underset{\sim}{\boldsymbol{C}^e} \cdot \frac{\partial g}{\partial(\boldsymbol{\sigma}-\boldsymbol{\alpha})} + \frac{\partial g}{\partial(\boldsymbol{\sigma}-\boldsymbol{\alpha})} : \frac{\partial \boldsymbol{\alpha}}{\partial \bar{\varepsilon}_p}. \tag{20}
$$

Note here that, for a given strain increment, the stress increment calculated by the asymmetric tangent modulus in Eq. (12) or Eq. (13) is the same as that calculated by the symmetric tangent modulus in Eq. (17) or Eq. (18) as rigorously proven in Appendix A. The symmetric tangent modulus can be implemented into a finite element analysis when the non-symmetric equation solver is not available. Also, the elasto-plastic tangent moduli are indifferent to the reference states of the yield stress function and the plastic potential because their gradients used in calculating the moduli are 0th order homogenous functions. Since the hardening is commonly described by the effective strain, Eqs. (12) and (17) are more convenient for numerical applications.

2.2. Hill (1948) yield function

Under the plane stress condition, the quadratic yield function proposed by Hill (1948) becomes

$$f^2 = (G+H)\sigma_{xx}^2 + (H+F)\sigma_{yy}^2 - 2H\sigma_{xx}\sigma_{yy} + 2N\sigma_{xy}^2 = \bar{\sigma}^2 \qquad (21)$$

where F, G, H and N are anisotropic coefficients and x, y and z are orthogonal principal anisotropic axes materially embedded along the rolling, transverse and thickness directions of sheets, respectively. The effective strain increment, $d\bar{\varepsilon}$, which is conjugate to Eq. (21) considering the plastic work equivalence principle, becomes

$$d\bar{\varepsilon}^2 = \frac{Fd\varepsilon_{xx}^2 + Gd\varepsilon_{yy}^2 + H(d\varepsilon_{xx}+d\varepsilon_{yy})^2}{FG+GH+HF} + \frac{2}{N}d\varepsilon_{xy}^2. \qquad (22)$$

Under the plane stress condition, the following relationships are obtained to calibrate the four anisotropic coefficients based on the yield stress along the rolling (x-) direction, σ_0, which is considered a reference (therefore, $G+H=1$) and three R-values (R_0, R_{90} and R_{45}, width-to-thickness strain ratio in the uni-axial tension test along the x, y and 45° directions, respectively):

$$F = \frac{R_0}{(1+R_0)R_{90}}, \quad G = \frac{1}{1+R_0}, \quad H = \frac{R_0}{1+R_0} \text{ and}$$
$$N = \frac{(1+2R_{45})(R_0+R_{90})}{2(1+R_0)R_{90}}. \qquad (23)$$

Also, the following relationships are obtained for four yield stresses when σ_0 is the reference value:

$$2F = \left(\frac{\sigma_0}{\sigma_{90}}\right)^2 - 1 + \left(\frac{\sigma_0}{\sigma_b}\right)^2, \qquad 2G = 1 - \left(\frac{\sigma_0}{\sigma_{90}}\right)^2 + \left(\frac{\sigma_0}{\sigma_b}\right)^2$$
$$2H = 1 + \left(\frac{\sigma_0}{\sigma_{90}}\right)^2 - \left(\frac{\sigma_0}{\sigma_b}\right)^2, \qquad 2N = \left(\frac{2\sigma_0}{\sigma_{45}}\right)^2 - \left(\frac{\sigma_0}{\sigma_b}\right)^2, \qquad (24)$$

where σ_0, σ_{90} and σ_{45} are yield stresses along the x, y and 45° directions, while σ_b is the balanced biaxial yield stress.

2.3. Yld2000-2d yield function

The plane stress yield stress function Yld2000-2d proposed by Barlat et al. (2003) is defined as

$$f = \left\{\frac{\phi'+\phi''}{2}\right\}^{\frac{1}{m}} = \bar{\sigma} \text{ with } \phi' = \left|\widetilde{S}_I' - \widetilde{S}_{II}'\right|^m \text{ and}$$
$$\phi'' = \left|2\widetilde{S}_{II}'' + \widetilde{S}_I''\right|^m + \left|2\widetilde{S}_{II}'' + \widetilde{S}_{II}''\right|^m, \qquad (25)$$

where $\widetilde{S}_k'$ and $\widetilde{S}_k''$ ($k = I, II$) are the principal values of the deviatoric stress tensor $\tilde{\mathbf{s}}$ ($\tilde{\mathbf{s}}'$ or $\tilde{\mathbf{s}}''$) modified by the following linear transformations:

$$\tilde{\mathbf{s}}' = \mathbf{C}' \cdot \mathbf{s} = \mathbf{C}' \cdot \mathbf{T} \cdot \boldsymbol{\sigma} = \mathbf{L}' \cdot \boldsymbol{\sigma},$$
$$\tilde{\mathbf{s}}'' = \mathbf{C}'' \cdot \mathbf{s} = \mathbf{C}'' \cdot \mathbf{T} \cdot \boldsymbol{\sigma} = \mathbf{L}'' \cdot \boldsymbol{\sigma}. \qquad (26)$$

Here, $\mathbf{C}'$ and $\mathbf{C}''$ (therefore, $\mathbf{L}'$ and $\mathbf{L}''$) contain eight independent anisotropic coefficients and $\mathbf{T}$ transforms the Cauchy stress tensor $\boldsymbol{\sigma}$ to its deviator $\mathbf{s}$; i.e.,

$$\mathbf{C}' = \begin{bmatrix} c_{11}' & 0 & 0 \\ 0 & c_{22}' & 0 \\ 0 & 0 & c_{66}' \end{bmatrix} \text{ and } \mathbf{C}'' = \begin{bmatrix} c_{11}'' & c_{12}'' & 0 \\ c_{21}'' & c_{22}'' & 0 \\ 0 & 0 & c_{66}'' \end{bmatrix}. \qquad (27)$$

3. Implicit numerical formulation

For the numerical formulation, the predictor–corrector scheme proposed by Chung (1984) and Simo and Hughes (1998) based on the incremental deformation plasticity theory (Chung and Richmond, 1993) was used in this work. Assuming elastic stress–strain relationship, the stress is initially updated for a given discrete strain increments, $\Delta\varepsilon_n$:

$$\boldsymbol{\sigma}_{n+1}^T = \boldsymbol{\sigma}_n + \underset{\sim}{\mathbf{C}}^e \cdot \Delta\varepsilon_n. \qquad (28)$$

where the superscript T denotes a trial state and the subscripts, n and $n+1$, denote the discretized process time step. Also, assuming purely (trial) elastic step, state variables are preserved from the previous step; i.e.,

$$\bar{\varepsilon}_{n+1}^T = \bar{\varepsilon}_n \text{ and } \boldsymbol{\alpha}_{n+1}^T = \boldsymbol{\alpha}_n. \qquad (29)$$

Then, the following yield condition is checked using the updated trial state variables:

$$f(\boldsymbol{\sigma}_{n+1}^T - \boldsymbol{\alpha}_{n+1}^T) - \bar{\sigma}_{iso}(\bar{\varepsilon}_{n+1}^T) < 0. \qquad (30)$$

If the yield condition is satisfied, the process at the $(n+1)$ th step is elastic. Otherwise, the step is elasto-plastic and the increment of the effective plastic strain, $\Delta\bar{\varepsilon}_{n+1}$, is iteratively obtained to satisfy the following consistency condition as explained next, in which the updated stress stays on the new yield surface:

$$\Phi_{n+1} = f(\boldsymbol{\sigma}_{n+1} - \boldsymbol{\alpha}_{n+1}) - \bar{\sigma}_{iso}(\bar{\varepsilon}_n + \Delta\bar{\varepsilon}_{n+1}) = 0. \qquad (31)$$

where

$$\boldsymbol{\sigma}_{n+1} = \boldsymbol{\sigma}_{n+1}^T - \underset{\sim}{\mathbf{C}}^e \cdot \frac{\partial g}{\partial(\boldsymbol{\sigma}_{n+\vartheta} - \boldsymbol{\alpha}_{n+\vartheta})} \frac{f(\boldsymbol{\sigma}_{n+\vartheta} - \boldsymbol{\alpha}_{n+\vartheta})}{g(\boldsymbol{\sigma}_{n+\vartheta} - \boldsymbol{\alpha}_{n+\vartheta})} \Delta\bar{\varepsilon}_{n+1} \qquad (32)$$

and

$$\boldsymbol{\alpha}_{n+1} = \boldsymbol{\alpha}_n + h_2(\bar{\varepsilon}_{n+\vartheta})\left[\frac{h_1(\bar{\varepsilon}_{n+\vartheta})}{h_2(\bar{\varepsilon}_{n+\vartheta})}\left(\frac{\boldsymbol{\sigma}_{n+\vartheta} - \boldsymbol{\alpha}_{n+\vartheta}}{\bar{\sigma}_{iso,n+\vartheta}}\right) - \boldsymbol{\alpha}_{n+\vartheta}\right]\Delta\bar{\varepsilon}_{n+1}. \qquad (33)$$

Here, the effective stress, $\bar{\sigma}_{iso}$, and the kinematic hardening parameters, h_1 and h_2, are prescribed values obtained from experiments, while ϑ is a design parameter (between 0.0 and 1.0), which defines the implicit algorithm.

3.1. Initialize state variables

At first, the trial state variables (including the trial stress) are taken as initial variables for a plastic corrector scheme; i.e.,

$$\boldsymbol{\sigma}_{n+1}^{k=1} = \boldsymbol{\sigma}_{n+1}^T,$$
$$\boldsymbol{\alpha}_{n+1}^{k=1} = \boldsymbol{\alpha}_{n+1}^T,$$
$$\bar{\varepsilon}_{n+1}^{k=1} = \bar{\varepsilon}_{n+1}^T,$$
$$\Delta\bar{\varepsilon}_{n+1}^{k=1} = \bar{\varepsilon}_{n+1}^{k=1} - \bar{\varepsilon}_n = 0. \qquad (34)$$

where the superscript, k, denotes the iteration number. Note here that the conjugate effective strain discrete increment, $\Delta\bar{\varepsilon}_p$, is updated from the relationship in Eq. (5).

3.2. Update the effective strain

In order to update the effective plastic strain, which satisfies the consistency condition in Eq. (31), the increment of the effective strain at the kth iteration is obtained by

$$\delta(\Delta\bar{\varepsilon}_{n+1})^{k+1} = -\frac{\Phi_{n+1}^k}{\left(\frac{\partial\Phi}{\partial\Delta\bar{\varepsilon}}\right)_{n+1}^k}, \qquad (35)$$

where

$$\Delta\bar{\varepsilon}_{n+1}^{k+1} = \Delta\bar{\varepsilon}_{n+1}^k + \delta(\Delta\bar{\varepsilon}_{n+1})^{k+1}. \qquad (36)$$

Here, by the chain rule, the linearized form of the denominator in Eq. (35) is

$$\left(\frac{\partial\Phi}{\partial\Delta\bar{\varepsilon}}\right)_{n+1}^k = \left(\frac{\partial\Phi}{\partial\boldsymbol{\sigma}}\right)_{n+1}^k \left(\frac{\partial\boldsymbol{\sigma}}{\partial\Delta\bar{\varepsilon}}\right)_{n+1}^k + \left(\frac{\partial\Phi}{\partial\boldsymbol{\alpha}}\right)_{n+1}^k \left(\frac{\partial\boldsymbol{\alpha}}{\partial\Delta\bar{\varepsilon}}\right)_{n+1}^k$$
$$+ \left(\frac{\partial\Phi}{\partial\bar{\sigma}_{iso}}\right)_{n+1}^k \left(\frac{\partial\bar{\sigma}_{iso}}{\partial\Delta\bar{\varepsilon}}\right)_{n+1}^k, \qquad (37)$$

where

$$\left(\frac{\partial \Phi}{\partial \boldsymbol{\sigma}}\right)_{n+1}^k = -\left(\frac{\partial \Phi}{\partial \boldsymbol{\alpha}}\right)_{n+1}^k = \frac{\partial f}{\partial (\boldsymbol{\sigma}_{n+\vartheta}^k - \boldsymbol{\alpha}_{n+\vartheta}^k)},$$
$$\left(\frac{\partial \Phi}{\partial \bar{\sigma}_{iso}}\right)_{n+1}^k = -1,$$
(38)

and

$$\left(\frac{\partial \boldsymbol{\sigma}}{\partial \Delta \bar{\varepsilon}}\right)_{n+1}^k = -\underset{\sim}{\mathbf{C}}^e \cdot \frac{\partial g}{\partial (\boldsymbol{\sigma}_{n+\vartheta}^k - \boldsymbol{\alpha}_{n+\vartheta}^k)} \frac{f(\boldsymbol{\sigma}_{n+\vartheta}^k - \boldsymbol{\alpha}_{n+\vartheta}^k)}{g(\boldsymbol{\sigma}_{n+\vartheta}^k - \boldsymbol{\alpha}_{n+\vartheta}^k)}.$$
(39)

Here, $\boldsymbol{\sigma}_{n+\vartheta}^k = \boldsymbol{\sigma}_n + \vartheta(\boldsymbol{\sigma}_{n+1}^k - \boldsymbol{\sigma}_n) = \boldsymbol{\sigma}_n + \vartheta \Delta \boldsymbol{\sigma}_n^k$ and $\boldsymbol{\alpha}_{n+\vartheta}^k = \boldsymbol{\alpha}_n + \vartheta(\boldsymbol{\alpha}_{n+1}^k - \boldsymbol{\alpha}_n) = \boldsymbol{\alpha}_n + \vartheta \Delta \boldsymbol{\alpha}_n^k$. Neglecting the second order variations for simplicity,

$$\left(\frac{\partial \boldsymbol{\alpha}}{\partial \Delta \bar{\varepsilon}}\right)_{n+1}^k = \bar{h}_2(\bar{\varepsilon}_{n+1}^k) \left[\frac{\bar{h}_1(\bar{\varepsilon}_{n+1}^k)}{\bar{h}_2(\bar{\varepsilon}_{n+1}^k)} \left(\frac{\boldsymbol{\sigma}_{n+1}^k - \boldsymbol{\alpha}_{n+1}^k}{\bar{\sigma}_{iso,n+1}^k(\boldsymbol{\sigma}_{n+1}^k - \boldsymbol{\alpha}_{n+1}^k)}\right) - \boldsymbol{\alpha}_{n+1}^k\right].$$
(40)

3.3. Update the stress

Then, the effective strain is updated by

$$\bar{\varepsilon}_{n+1}^{k+1} = \bar{\varepsilon}_n + \Delta \bar{\varepsilon}_{n+1}^{k+1} = \bar{\varepsilon}_{n+1}^k + \delta(\Delta \bar{\varepsilon}_{n+1})^{k+1},$$
$$\bar{\varepsilon}_{n+\vartheta}^{k+1} = \bar{\varepsilon}_n + \vartheta(\bar{\varepsilon}_{n+1}^{k+1} - \bar{\varepsilon}_n) = \bar{\varepsilon}_n + \vartheta \Delta \bar{\varepsilon}_{n+1}^{k+1},$$
(41)

while the stress is updated by

$$\boldsymbol{\sigma}_{n+1}^{k+1} = \boldsymbol{\sigma}_{n+1}^1 - \underset{\sim}{\mathbf{C}}^e \cdot \Delta \boldsymbol{\varepsilon}_{n+1}^{p,k+1},$$
$$\boldsymbol{\sigma}_{n+\vartheta}^{k+1} = \boldsymbol{\sigma}_n + \vartheta(\boldsymbol{\sigma}_{n+1}^{k+1} - \boldsymbol{\sigma}_n) = \boldsymbol{\sigma}_n + \vartheta \Delta \boldsymbol{\sigma}_n^{k+1}.$$
(42)

Here,

$$\Delta \boldsymbol{\varepsilon}_{n+1}^{p,k+1} = \frac{\partial g}{\partial (\boldsymbol{\sigma}_{n+\vartheta}^k - \boldsymbol{\alpha}_{n+\vartheta}^k)} \frac{f(\boldsymbol{\sigma}_{n+\vartheta}^k - \boldsymbol{\alpha}_{n+\vartheta}^k)}{g(\boldsymbol{\sigma}_{n+\vartheta}^k - \boldsymbol{\alpha}_{n+\vartheta}^k)} \Delta \bar{\varepsilon}_{n+1}^{k+1}$$
(43)

Therefore, Eq. (42) becomes,

$$\boldsymbol{\sigma}_{n+1}^{k+1} = \boldsymbol{\sigma}_{n+1}^1 - \underset{\sim}{\mathbf{C}}^e \cdot \frac{\partial g}{\partial (\boldsymbol{\sigma}_{n+\vartheta}^k - \boldsymbol{\alpha}_{n+\vartheta}^k)} \frac{f(\boldsymbol{\sigma}_{n+\vartheta}^k - \boldsymbol{\alpha}_{n+\vartheta}^k)}{g(\boldsymbol{\sigma}_{n+\vartheta}^k - \boldsymbol{\alpha}_{n+\vartheta}^k)} \Delta \bar{\varepsilon}_{n+1}^{k+1}.$$
(44)

3.4. Update state variables and confirmation of the consistency condition

From the updated effective plastic strain, the back-stress is updated by

$$\boldsymbol{\alpha}_{n+1}^{k+1} = \boldsymbol{\alpha}_n + h_2(\bar{\varepsilon}_{n+\vartheta}^k) \left[\frac{h_1(\bar{\varepsilon}_{n+\vartheta}^k)}{h_2(\bar{\varepsilon}_{n+\vartheta}^k)} \left(\frac{\boldsymbol{\sigma}_{n+\vartheta}^k - \boldsymbol{\alpha}_{n+\vartheta}^k}{\bar{\sigma}_{iso,n+\vartheta}^k}\right) - \boldsymbol{\alpha}_{n+\vartheta}^k\right] \Delta \bar{\varepsilon}_{n+1}^{k+1},$$
$$\boldsymbol{\alpha}_{n+\vartheta}^{k+1} = \boldsymbol{\alpha}_n + \vartheta(\boldsymbol{\alpha}_{n+1}^{k+1} - \boldsymbol{\alpha}_n) = \boldsymbol{\alpha}_n + \vartheta \Delta \boldsymbol{\alpha}_n^{k+1}.$$
(45)

And then, the satisfaction of the consistency condition is confirmed:

$$\Phi_{n+1}^{k+1} = f(\boldsymbol{\sigma}_{n+1}^{k+1} - \boldsymbol{\alpha}_{n+1}^{k+1}) - \bar{\sigma}_{iso}(\bar{\varepsilon}_{n+1}^{k+1}) = 0$$
(46)

If the condition is violated, updating the iteration number, $k = k + 1$, repeat the above scheme, from Section 3.2–3.4, until the consistency condition is satisfied. After satisfaction of the condition, the tangent stiffness modulus should be calculated using one of Eqs. (12), (13), (17) and (18) for implicit analysis to obtain the strain increment balancing the moment equation under a specific boundary condition.

4. Material characterization

In this work, AA2090-T3 sheets with 1.6 mm thickness and AA5042 sheets with 0.208 mm thickness were considered. The mechanical properties of AA2090-T3 have been referred in the previous works by Chung et al. (1996, 1997, 2011) and Yoon et al. (2000, 2006, 2011), while those of AA5042 have been provided by the benchmark problem of the NUMISHEET 2011 conference (Yoon and Dick, 2011).

4.1. Coefficients of plastic potential and yield stress function

The eight yield stresses and eight R-values of each material measured for the simple tension test and the balanced biaxial tensile tension test are summarized in Tables 1 and 2. In order to incorporate anisotropy, the Yld2000-2d function was applied both for the plastic potential (for R-values) and the yield stress function (for yield stresses) based on the non-associated flow rule in this work and its performance was compared with that of the non-associated model based on the (Hill, 1948) function. Note that simple tension in the rolling direction was considered the reference state throughout this characterization work.

For the (Hill, 1948) function under the plane stress condition, the anisotropy coefficients of the yield function, f, were determined by using the equations shown in Eq. (24), while those of the plastic potential, g, were determined from Eq. (23). The resulting coefficients of each material are listed in Table 3.

As for the Yld2000-2d function, the eight anisotropic coefficients of the yield function, f, were determined by eight mechanical measurements, σ_0, σ_{15}, σ_{30}, σ_{45}, σ_{60}, σ_{75}, σ_{90} and σ_b, which are yield stresses obtained in simple tension at 0°, 15°, 30°, 45°, 60°, 75° and 90° to the rolling (x-) direction as well as yield stress under the balanced biaxial tension condition, respectively. The coefficients in the plastic potential, g, were determined by eight mechanical measurements, R_0, R_{15}, R_{30}, R_{45}, R_{60}, R_{75}, R_{90} and R_b, which are R-values obtained in simple tension at 0°, 15°, 30°, 45°, 60°, 75° and 90° to the rolling (x-) direction as well as in-plane principal strain ratio under balanced biaxial tension, respectively (see Appendix B for the characterization procedure). For convenience, the eight independent coefficients α_i ($i = 1 \sim 8$) were defined, replacing eight components of $\mathbf{C}'$ and $\mathbf{C}''$ in Eq. (27), as

$$
\begin{bmatrix} L'_{11} \\ L'_{12} \\ L'_{21} \\ L'_{22} \\ L'_{66} \end{bmatrix} = \begin{bmatrix} 2/3 & 0 & 0 \\ -1/3 & 0 & 0 \\ 0 & -1/3 & 0 \\ 0 & 2/3 & 0 \\ 0 & 0 & 1 \end{bmatrix} \begin{bmatrix} \alpha_1 \\ \alpha_2 \\ \alpha_7 \end{bmatrix},
$$
$$
\begin{bmatrix} L''_{11} \\ L''_{12} \\ L''_{21} \\ L''_{22} \\ L''_{66} \end{bmatrix} = \frac{1}{9} \begin{bmatrix} -2 & 2 & 8 & -2 & 0 \\ 1 & -4 & -4 & 4 & 0 \\ 4 & -4 & -4 & 1 & 0 \\ -2 & 8 & 2 & -2 & 0 \\ 0 & 0 & 0 & 0 & 9 \end{bmatrix} \begin{bmatrix} \alpha_3 \\ \alpha_4 \\ \alpha_5 \\ \alpha_6 \\ \alpha_8 \end{bmatrix},
$$
(47)

such that isotropy is recovered when unit values are assigned for each α_i. Resulting coefficients of each material are listed in Table 4. Here, the anisotropic coefficients of the Yld2000-2d function for the associated flow model determined by eight anisotropic measurements, σ_0, σ_{45}, σ_{90}, R_0, R_{45}, R_{90}, σ_b and R_b are also summarized for comparison.

Calculated simple tension yield stresses and R-values based on the resulting yield functions and plastic potentials for AA2090-T3 and AA5042 are compared with experiments in Figs. 2 and 3, while yield stress function and plastic potential contours are shown in Figs. 4 and 5, respectively. Distributions of the calculated R-values

Table 1
Normalized initial yield stresses of AA2090-T3 and AA5042.

	σ_0/σ_0	σ_{15}/σ_0	σ_{30}/σ_0	σ_{45}/σ_0	σ_{60}/σ_0	σ_{75}/σ_0	σ_{90}/σ_0	σ_b/σ_0
AA2090-T3	1.0000	0.9605	0.9102	0.8114	0.8096	0.8815	0.9102	1.035
AA5042	1.0000	1.0000	1.0174	1.0149	1.0174	1.0373	1.0448	1.1090

Table 2
R-values of AA2090-T3 and AA5042.

	R_0	R_{15}	R_{30}	R_{45}	R_{60}	R_{75}	R_{90}	R_b
AA2090-T3	0.2115	0.3269	0.6923	1.5769	1.0385	0.5384	0.6923	0.67
AA5042	0.384	0.1920	0.650	0.860	1.299	1.224	1.436	0.991

Table 3
Anisotropic coefficients of the Hill (1948) function for AA2090-T3 and AA5042.

	F	G	H	N
AA2090-T3				
Yield *f*	0.6035	0.3965	0.6035	2.538
Potential *g*	0.2522	0.8254	0.1746	2.238
AA5042				
Yield *f*	0.3946	0.4485	0.5515	1.5350
Potential *g*	0.1873	0.7386	0.2614	1.4526

and normalized initial yield stresses confirm that the non-associated model based on the Yld2000-2d function well captures the anisotropy of three materials under the uniaxial and biaxial tensile conditions.

4.2. Isotropic/isotropic-kinematic hardening parameters

For the uni-axial (monotonously proportional) deformation, the following relationship is valid:

$$\bar{\sigma} = \bar{\sigma}_{iso} + \bar{\alpha} = \bar{\sigma}_{iso}(\bar{\varepsilon} = 0) + [\bar{\sigma}_{iso} - \bar{\sigma}_{iso}(\bar{\varepsilon} = 0)] + \bar{\alpha},$$
$$\mathrm{d}\bar{\sigma} = \mathrm{d}\bar{\sigma}_{iso} + \mathrm{d}\bar{\alpha} = \varphi\mathrm{d}\bar{\sigma} + (1 - \varphi)\mathrm{d}\bar{\sigma}, \quad 0 \leqslant \varphi \leqslant 1. \tag{48}$$

Here, $\bar{\sigma}_{iso}$ is the size of the yield stress function (equivalently, difference between the yield stress and the back stress in the rolling direction as a reference state), $\bar{\alpha}$ is the effective quantity of the back-stress obtained from the yield stress function by replacing $\boldsymbol{\sigma} - \boldsymbol{\alpha}$ with $\boldsymbol{\alpha}$, (equivalently, the back-stress in the rolling direction), while φ is a parameter to determine the ratio between the isotropic hardening increment and the back-stress increment. For general deformation including non-monotonous deformation cases, φ should be characterized through various non-monotonous experiments (since φ does not affect hardening for monotonously proportional loading). However, only monotonously proportional data were available in this work; therefore, the parameter, φ, was assumed 0.0 (full isotropic hardening), 0.5 and 1.0 (full kinematic hardening) initially for comparison purposes and it was confirmed that φ insignificantly affected the earring profiles so that the results of $\varphi = 0.5$ are reported here; i.e.,

$$\bar{\sigma}_{iso} = \bar{\sigma}_{iso}(0) + \Delta\bar{\sigma}_{iso} = \bar{\sigma}(0) + 0.5[\bar{\sigma} - \bar{\sigma}(0)]$$
$$\bar{\alpha} = \bar{\alpha}(0) + \Delta\bar{\alpha} = 0.5[\bar{\sigma} - \bar{\sigma}(0)], \tag{49}$$

where $\bar{\sigma}_{iso}(0) = \bar{\sigma}(0)$ and $\bar{\alpha}(0) = 0$. Based on the measured hardening curves of each material, the isotropic hardening and kinematic hardening laws were obtained using Eq. (49) as summarized in Table 5. Eq. (9), when applied for the reference state, becomes the first order differential equation, $\mathrm{d}\bar{\alpha}/\mathrm{d}\bar{\varepsilon} = h_1 - h_2\bar{\alpha}$, whose solution is

$$\bar{\alpha} = \frac{h_1}{h_2}(1 - e^{-h_2\bar{\varepsilon}}). \tag{50}$$

Using the obtained kinematic hardening laws in Table 5, the kinematic hardening parameters, h_1 and h_2, were obtained for each material as summarized in Table 6.
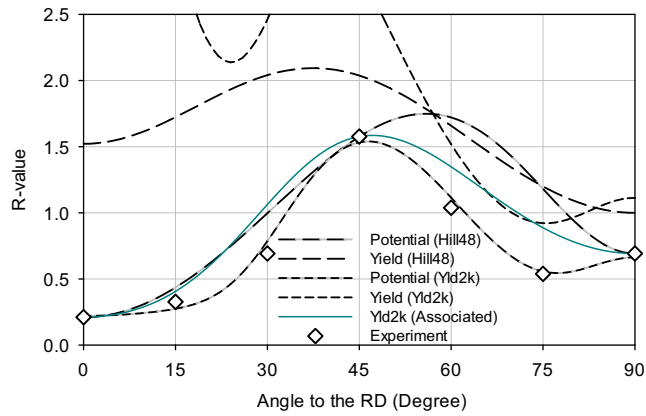
5. Cylindrical cup drawing simulation

The non-associated flow rule and characterized material properties were implemented into the commercial FE program ABAQUS/Explicit with the aid of user defined material subroutine. And then, for verification purposes, the developed constitutive model was applied for the simulation of cylindrical cup drawing tests. Schematic views of tools are shown in Fig. 6, while their dimensions are summarized in Table 7. Note that the radius of the die profile, Rd, for AA2090-T3 was slightly modified to 51.24 mm from that used for experiments (50.74 mm) to accommodate severe thickening in simulation results of the non-associated model with (Hill, 1948) function.

In the simulations, the tool surfaces were modeled by analytical rigid surfaces and the blank was modeled with 4-noded shell elements with reduced volume integration (S4R) and with 9 integration points through the thickness. For AA2090-T3, the element size of the blank was approximately 1.0 mm × 1.0 mm except for the center region as shown in Fig. 7(a), while those for AA5042 were approximately 0.4 mm × 0.4 mm considering the die corner profile radius, rp, as shown in Fig. 7(b). A blank holding force of 22.2 kN (for AA2090-T3) and 8.9 kN (for AA5042) was maintained throughout the simulation and the friction coefficient was assumed to be a constant of 0.005 for all materials. Ignoring strain rate sensitivity, the dynamic analysis, ABAQUS/Explicit, was applied for simulations. Young's modulus, Poisson's ratio and density used for simulations for each material were 68.9 GPa, 0.33 and 2.72 g/cm³, respectively.
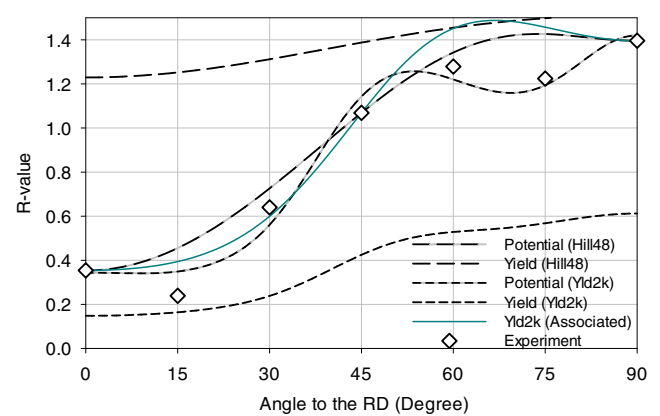
As for the material models, the developed non-associated models based on the (Hill, 1948) and Yld2000 functions were used for each material as well as the associated model based on the Yld2000 yield function. Here, the isotropic-kinematic hardening was applied for each material model with $\varphi = 0.5$ as an example. In Figs. 8 and 9, the simulated earing profiles are compared with experiments. The simulation results based on the non-associated flow model with the Yld2000 function successfully predicted 6 and 8 ears measured in the cylindrical cup drawing tests for AA2090-T3 and AA5042, respectively, while those based on the non-associated flow model with the (Hill, 1948) function and the associated model with the Yld2000 yield function predicted only 4 ears for each material. Even the earing profiles have good agreement in particular for AA5042, while some discrepancy observed for AA2090-T3 for heights at 0°, 180° and 360°. However, for an orthotropic material, the reflection of earing profile between 0° and 90° with respect to the 90° axis is supposed to coincide with the profile between 90° and 180°. But, the measured earing profile for AA2090-T3 shown in Fig. 8 does not comply well with this

Table 4
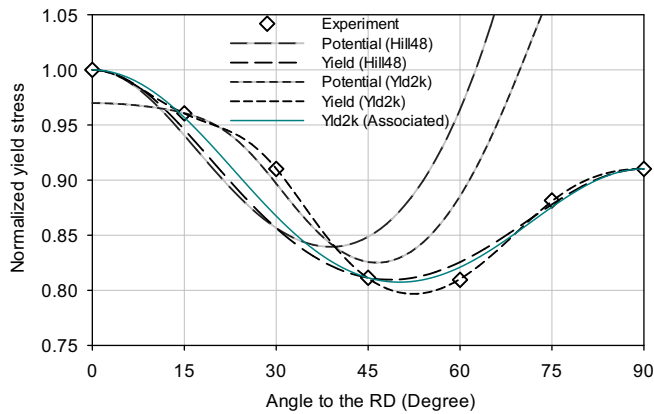Anisotropic coefficients of Yld2000-2d function for AA2090-T3 and AA5042.

	m	α_1	α_2	α_3	α_4	α_5	α_6	α_7	α_8
AA2090-T3									
Yield f	8	−0.7128	2.0368	1.6288	0.6895	0.5524	−1.0570	1.2545	1.2626
Potential g	8	−1.2694	1.7314	−0.0734	0.6589	1.0234	0.7210	1.1688	1.5449
Associated	8	0.4878	1.3773	0.7539	1.0245	1.0362	0.9037	1.2314	1.4849
AA5042									
Yield f	8	−0.8052	1.6285	0.1199	0.7976	1.0216	0.8131	0.7547	1.3230
Potential g	14	−1.2243	1.8246	−1.0709	0.3568	1.0023	0.9091	0.9997	1.8108
Associated	8	0.4489	1.2811	1.0174	0.8894	0.9738	0.6454	0.9735	1.0775

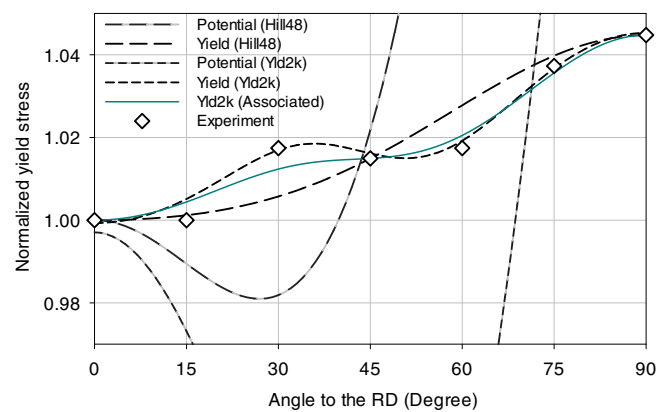**Fig. 2.** Anisotropy of plastic potential/yield functions based on the Hill and Yld2000-2d functions for AA2090-T3: (a) R-value distributions and (b) normalized stress distributions.

Fig. 3. Anisotropy of plastic potential/yield functions based on the Hill and Yld2000-2d functions for AA5042: (a) R-value distributions and (b) normalized stress distributions.

condition, which might suggest slight error in the measurement (Chung et al., 1997).

6. Summary

A constitutive formulation to represent the planar anisotropy of sheets based on the non-associated flow rule was developed under the isotropic-kinematic hardening framework (Chung et al., 2005) for generalization purposes along with its numerical formulation for the finite element method. Besides the asymmetric stiffness modulus, the symmetric stiffness modulus was successfully derived in this work, which would significantly improve numerical efficiency. In order to simulate 6 and 8 ears, respectively for

AA2090-T3 and AA5042 sheets, observed in the circular cylindrical cup drawing test, the non-quadratic function Yld2000-2d proposed by Barlat et al. (2003) was applied for the plastic potential and the yield stress function in this work, which successfully predicted 6 and 8 ears, respectively.
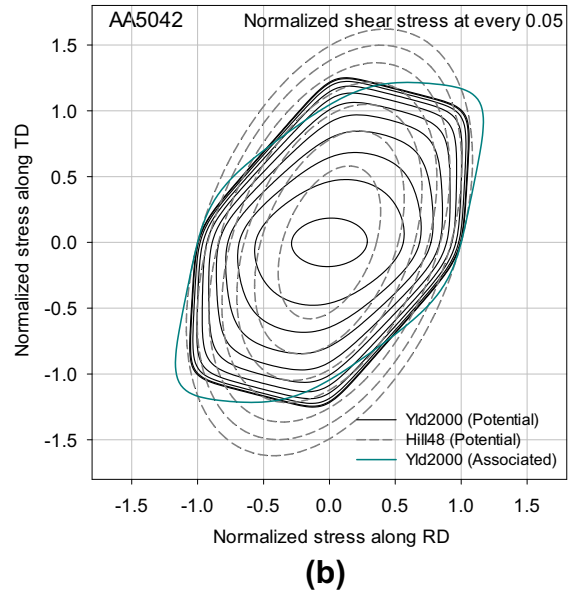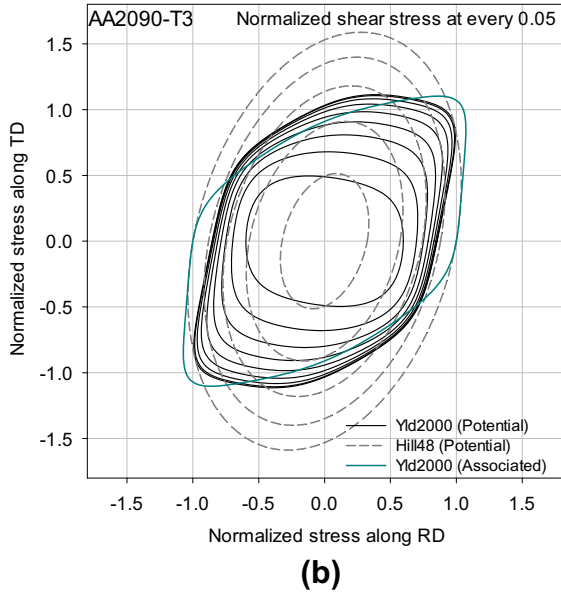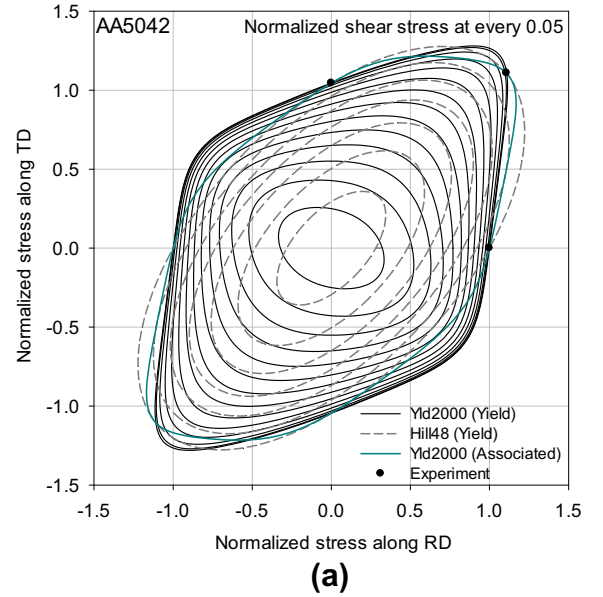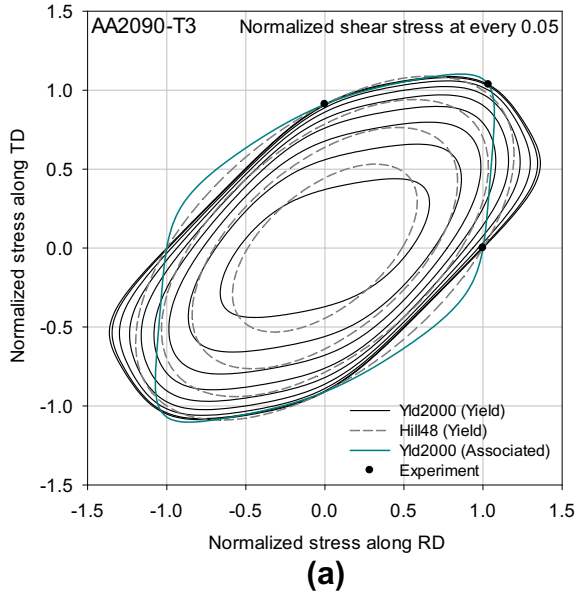
Fig. 4. Contours based on the Hill and Yld2000 functions for AA2090-T3: (a) yield functions and (b) plastic potentials.

Fig. 5. Contours based on the Hill and Yld2000 functions for AA5042: (a) yield functions and (b) plastic potentials.

Appendix A. Asymmetric and symmetric tangent moduli of the non-associated flow rule

The stress increment for a given strain increment based on Eq. (12) for the asymmetric modulus is,

$$d\boldsymbol{\sigma} = \underset{\sim}{\boldsymbol{C}}^e \cdot d\boldsymbol{\varepsilon} - \frac{\frac{f(\boldsymbol{\sigma}-\boldsymbol{\alpha})}{g(\boldsymbol{\sigma}-\boldsymbol{\alpha})}\underset{\sim}{\boldsymbol{C}}^e : \frac{\partial g}{\partial(\boldsymbol{\sigma}-\boldsymbol{\alpha})} \otimes \frac{\partial f}{\partial(\boldsymbol{\sigma}-\boldsymbol{\alpha})} : \underset{\sim}{\boldsymbol{C}}^e \cdot d\boldsymbol{\varepsilon}}{\frac{f(\boldsymbol{\sigma}-\boldsymbol{\alpha})}{g(\boldsymbol{\sigma}-\boldsymbol{\alpha})}\frac{\partial f}{\partial(\boldsymbol{\sigma}-\boldsymbol{\alpha})} : \underset{\sim}{\boldsymbol{C}}^e \cdot \frac{\partial g}{\partial(\boldsymbol{\sigma}-\boldsymbol{\alpha})} + \frac{\partial f}{\partial(\boldsymbol{\sigma}-\boldsymbol{\alpha})} : \frac{\partial \boldsymbol{\alpha}}{\partial \bar{\varepsilon}} + \frac{\partial \bar{\sigma}_{iso}}{\partial \bar{\varepsilon}}}, \quad (A.1)$$

while that based on Eq. (17) for the symmetric modulus is,

$$d\boldsymbol{\sigma} = \underset{\sim}{\boldsymbol{C}}^e \cdot d\boldsymbol{\varepsilon} - \frac{\frac{f(\boldsymbol{\sigma}-\boldsymbol{\alpha})}{g(\boldsymbol{\sigma}-\boldsymbol{\alpha})}\underset{\sim}{\boldsymbol{C}}^e : \frac{\partial g}{\partial(\boldsymbol{\sigma}-\boldsymbol{\alpha})} \otimes \frac{\partial g}{\partial(\boldsymbol{\sigma}-\boldsymbol{\alpha})} : \underset{\sim}{\boldsymbol{C}}^e \cdot d\boldsymbol{\varepsilon}}{\frac{f(\boldsymbol{\sigma}-\boldsymbol{\alpha})}{g(\boldsymbol{\sigma}-\boldsymbol{\alpha})}\frac{\partial g}{\partial(\boldsymbol{\sigma}-\boldsymbol{\alpha})} : \underset{\sim}{\boldsymbol{C}}^e \cdot \frac{\partial g}{\partial(\boldsymbol{\sigma}-\boldsymbol{\alpha})} + \frac{\partial g}{\partial(\boldsymbol{\sigma}-\boldsymbol{\alpha})} : \frac{\partial \boldsymbol{\alpha}}{\partial \bar{\varepsilon}} + \frac{\partial \bar{\sigma}_{pot}}{\partial \bar{\varepsilon}}}. \quad (A.2)$$

Then, the difference between the stress increments in Eqs. (A.1) and (A.2) is, after considering Eqs. (10) and (15),

$$\Delta d\boldsymbol{\sigma} = -\frac{\frac{f(\boldsymbol{\sigma}-\boldsymbol{\alpha})}{g(\boldsymbol{\sigma}-\boldsymbol{\alpha})}\underset{\sim}{\boldsymbol{C}}^e : \frac{\partial g}{\partial(\boldsymbol{\sigma}-\boldsymbol{\alpha})} \otimes \frac{\partial f}{\partial(\boldsymbol{\sigma}-\boldsymbol{\alpha})} : \underset{\sim}{\boldsymbol{C}}^e \cdot d\boldsymbol{\varepsilon}}{\frac{f(\boldsymbol{\sigma}-\boldsymbol{\alpha})}{g(\boldsymbol{\sigma}-\boldsymbol{\alpha})}\frac{\partial f}{\partial(\boldsymbol{\sigma}-\boldsymbol{\alpha})} : \underset{\sim}{\boldsymbol{C}}^e \cdot \frac{\partial g}{\partial(\boldsymbol{\sigma}-\boldsymbol{\alpha})} + \frac{\partial f}{\partial(\boldsymbol{\sigma}-\boldsymbol{\alpha})} : \frac{\partial \boldsymbol{\alpha}}{\partial \bar{\varepsilon}} + \frac{\partial \bar{\sigma}_{iso}}{\partial \bar{\varepsilon}}}$$

$$+ \frac{\frac{f(\boldsymbol{\sigma}-\boldsymbol{\alpha})}{g(\boldsymbol{\sigma}-\boldsymbol{\alpha})}\underset{\sim}{\boldsymbol{C}}^e : \frac{\partial g}{\partial(\boldsymbol{\sigma}-\boldsymbol{\alpha})} \otimes \frac{\partial g}{\partial(\boldsymbol{\sigma}-\boldsymbol{\alpha})} : \underset{\sim}{\boldsymbol{C}}^e \cdot d\boldsymbol{\varepsilon}}{\frac{\partial g}{\partial(\boldsymbol{\sigma}-\boldsymbol{\alpha})}:\underset{\sim}{\boldsymbol{C}}^e \cdot d\boldsymbol{\varepsilon}} \left(\frac{f(\boldsymbol{\sigma}-\boldsymbol{\alpha})}{g(\boldsymbol{\sigma}-\boldsymbol{\alpha})}\frac{\partial f}{\partial(\boldsymbol{\sigma}-\boldsymbol{\alpha})} : \underset{\sim}{\boldsymbol{C}}^e \cdot \frac{\partial g}{\partial(\boldsymbol{\sigma}-\boldsymbol{\alpha})} + \frac{\partial f}{\partial(\boldsymbol{\sigma}-\boldsymbol{\alpha})} : \frac{\partial \boldsymbol{\alpha}}{\partial \bar{\varepsilon}} + \frac{\partial \bar{\sigma}_{iso}}{\partial \bar{\varepsilon}} \right)} = \frac{f(\boldsymbol{\sigma}-\boldsymbol{\alpha})}{g(\boldsymbol{\sigma}-\boldsymbol{\alpha})}\underset{\sim}{\boldsymbol{C}}^e$$

$$: \frac{\partial g}{\partial(\boldsymbol{\sigma}-\boldsymbol{\alpha})} \left[\frac{\frac{\partial f}{\partial(\boldsymbol{\sigma}-\boldsymbol{\alpha})}:\underset{\sim}{\boldsymbol{C}}^e \cdot d\boldsymbol{\varepsilon}}{\frac{\partial g}{\partial(\boldsymbol{\sigma}-\boldsymbol{\alpha})}:\underset{\sim}{\boldsymbol{C}}^e \cdot d\boldsymbol{\varepsilon}}\frac{\partial g}{\partial(\boldsymbol{\sigma}-\boldsymbol{\alpha})} : \underset{\sim}{\boldsymbol{C}}^e \cdot d\boldsymbol{\varepsilon} - \frac{\partial f}{\partial(\boldsymbol{\sigma}-\boldsymbol{\alpha})} : \underset{\sim}{\boldsymbol{C}}^e \cdot d\boldsymbol{\varepsilon}}{\frac{f(\boldsymbol{\sigma}-\boldsymbol{\alpha})}{g(\boldsymbol{\sigma}-\boldsymbol{\alpha})}\frac{\partial f}{\partial(\boldsymbol{\sigma}-\boldsymbol{\alpha})} : \underset{\sim}{\boldsymbol{C}}^e \cdot \frac{\partial g}{\partial(\boldsymbol{\sigma}-\boldsymbol{\alpha})} + \frac{\partial f}{\partial(\boldsymbol{\sigma}-\boldsymbol{\alpha})} : \frac{\partial \boldsymbol{\alpha}}{\partial \bar{\varepsilon}} + \frac{\partial \bar{\sigma}_{iso}}{\partial \bar{\varepsilon}}} \right] = \boldsymbol{0} \quad (A.3)$$

Appendix B. Characterization of Yld2000-2d coefficients

A procedure for the characterization of the eight anisotropy coefficients for the Yld2000-2d function based on eight measured properties such as initial yield stress or R-value is summarized

Table 5
Isotropic/isotropic-kinematic hardening laws for AA2090-T3 and AA5042.

	$\bar{\sigma}$ (MPa)	σ_{iso} (MPa)	$\bar{\alpha}$ (MPa)
AA2090-T3	$646(0.025 + \bar{\varepsilon})^{0.227}$	$323(0.025 + \bar{\varepsilon})^{0.227} + 139.81$	$323(0.025 + \bar{\varepsilon})^{0.227} - 139.81$
AA5042	$375.08 - 107.28e^{-17.859\bar{\varepsilon}}$	$321.44 - 53.64e^{-17.859\bar{\varepsilon}}$	$53.64 - 53.64e^{-17.859\bar{\varepsilon}}$

Table 6
Kinematic hardening parameters for AA2090-T3 and AA5042.

	h_1 (MPa)	h_2
AA2090-T3	1057.15	11.898
AA5042	957.957	17.859

Fig. 6. Schematic view of tools for (a) AA2090-T3 and (b) AA5042.

here. In order to determine the convergence of the anisotropy coefficients $\alpha_i (i = 1 \sim 8)$, the following condition is applied during iteration:

$$\widetilde{R} = \sum_{j=1}^{8} w_j R_j^2 \leqslant TOL \tag{A.4}$$

where $\widetilde{R}$ is the total residual, R_j is the residual value for the jth condition (or measurement), w_j is the weight factor for each condition, TOL is tolerance. If the total residual, $\widetilde{R}$, is greater than the tolerance, TOL, the increments of the anisotropy coefficients are updated based on the Newton–Raphson method until the following condition is satisfied:

$$\widetilde{R}^{k+1} = \sum_{j=1}^{8} w_j \left(R_j^k + \Delta R_j^{k+1} \right)^2 \leqslant TOL. \tag{A.5}$$

Here, k denotes the iteration number, while the anisotropy coefficients are updated by

$$\alpha_i^{k+1} = \alpha_i^k + \Delta\alpha_i^{k+1} = \alpha_i^k - \left(\frac{\partial R_j}{\partial \alpha_i} \right)^{-1} R_j^k. \tag{A.6}$$

For the measured (initial) yield stress, the following equation should be satisfied:

$$R_F = \bar{\sigma}(\widehat{\boldsymbol{\sigma}}) - \bar{\sigma} = \left(\frac{\phi(\widehat{\boldsymbol{\sigma}})}{2} \right)^{\frac{1}{m}} - \bar{\sigma} = 0, \tag{A.7}$$

where $\bar{\sigma}$ is the (initial) effective yield stress and $\widehat{\boldsymbol{\sigma}}$ is the (initial) yield stress components based on the reference coordinate system (which is aligned along the rolling direction in this work). The stress components for the reference coordinate system are obtained from the following equation

$$\widehat{\boldsymbol{\sigma}} = \begin{bmatrix} \sigma_{xx} \\ \sigma_{yy} \\ \sigma_{xy} \end{bmatrix} = \begin{bmatrix} \cos^2\theta & \sin^2\theta & -2\cos\theta\sin\theta \\ \sin^2\theta & \cos^2\theta & 2\cos\theta\sin\theta \\ \cos\theta\sin\theta & -\cos\theta\sin\theta & \cos^2\theta - \sin^2\theta \end{bmatrix} \begin{bmatrix} \sigma_{11} \\ \sigma_{22} \\ \sigma_{12} \end{bmatrix}. \tag{A.8}$$

Here, σ_{11}, σ_{12} and σ_{22}, are the stress components for the coordinate system rotated θ degrees from the reference configuration as shown in Fig. B.1. For instance, σ_{11}, σ_{22} and σ_{12} are σ_θ, 0 and 0 for the simple tension, while σ_{11}, σ_{12} and σ_{22} are σ_b, σ_b and 0 for the balanced biaxial tension.

As for the measured R-value, the following equations should be satisfied for the simple tension conditions and balanced biaxial condition, respectively:

$$R_{G,ST} = \frac{\frac{\partial\bar{\sigma}(\widehat{\boldsymbol{\sigma}})}{\partial\sigma_{22}}}{\frac{\partial\bar{\sigma}(\widehat{\boldsymbol{\sigma}})}{\partial\sigma_{33}}} - R_{ST} = -\frac{\frac{\partial\phi(\widehat{\boldsymbol{\sigma}})}{\partial\sigma_{22}}}{\frac{\partial\phi(\widehat{\boldsymbol{\sigma}})}{\partial\sigma_{11}} + \frac{\partial\phi(\widehat{\boldsymbol{\sigma}})}{\partial\sigma_{22}}} - R_{ST} = 0, \tag{A.9}$$

$$R_{G,BB} = \frac{\frac{\partial\bar{\sigma}(\widehat{\boldsymbol{\sigma}})}{\partial\sigma_{11}}}{\frac{\partial\bar{\sigma}(\widehat{\boldsymbol{\sigma}})}{\partial\sigma_{22}}} - R_{BB} = \frac{\frac{\partial\phi(\widehat{\boldsymbol{\sigma}})}{\partial\sigma_{11}}}{\frac{\partial\phi(\widehat{\boldsymbol{\sigma}})}{\partial\sigma_{22}}} - R_{BB} = 0. \tag{A.10}$$

In this work, the condition in Eq. (A.7) was used for the characterization of the yield function, while the conditions in Eqs. (A.9) and (A.10) were utilized for the characterization of the plastic potential function.

The derivatives, $\frac{\partial\bar{\sigma}(\boldsymbol{\sigma})}{\partial\boldsymbol{\sigma}}$, are obtained by applying the chain rules; i.e.,

$$\left[\frac{\partial\bar{\sigma}(\widehat{\boldsymbol{\sigma}})}{\partial\boldsymbol{\sigma}} \right] = \begin{bmatrix} \frac{\partial\bar{\sigma}(\widehat{\boldsymbol{\sigma}})}{\partial\sigma_{11}} \\ \frac{\partial\bar{\sigma}(\widehat{\boldsymbol{\sigma}})}{\partial\sigma_{22}} \\ \frac{\partial\bar{\sigma}(\widehat{\boldsymbol{\sigma}})}{\partial\sigma_{12}} \end{bmatrix} = \left[\frac{\partial\bar{\sigma}(\widehat{\boldsymbol{\sigma}})}{\partial\phi'} \frac{\partial\phi'}{\partial\tilde{s}'} \frac{\partial\tilde{s}'}{\partial s'} \frac{\partial s'}{\partial\widehat{\boldsymbol{\sigma}}} \frac{\partial\widehat{\boldsymbol{\sigma}}}{\partial\boldsymbol{\sigma}} + \frac{\partial\bar{\sigma}(\boldsymbol{\sigma})}{\partial\phi''} \frac{\partial\phi''}{\partial\tilde{s}''} \frac{\partial\tilde{s}''}{\partial s''} \frac{\partial s''}{\partial\widehat{\boldsymbol{\sigma}}} \frac{\partial\widehat{\boldsymbol{\sigma}}}{\partial\boldsymbol{\sigma}} \right], \tag{A.11}$$

where $\tilde{s}'$ and $\tilde{s}''$ are principal values of the deviatoric stress tensors, s' and s'', respectively, while $\boldsymbol{\sigma}$ and $\widehat{\boldsymbol{\sigma}}$ are stress components of the θ degree rotated configuration and the reference configuration, respectively. Here,

Table 7
Dimensions of tools for AA2090-T3 and AA5042 (unit: mm).

	Rp	Rd	Rh	Rb	rp	rd	H1	a1 (degree)
AA2090-T3	48.73	51.24	51.24	79.38	12.70	12.70	–	–
AA5042	22.860	23.368	23.114	38.062	2.229	1.905	12.7	1.905

(a)

(b)

Fig. 7. Blank Meshes for (a) AA2090-T3 and (b) AA5042.

(a)

(b)

Fig. 8. Comparison of measured and calculated earing profiles of AA2090-T3: (a) based on the non-associated model with Hill48 and the associated model with Yld2000, (b) based on the non-associated model with Yld2000.

$$\frac{\partial \bar{\sigma}(\widehat{\boldsymbol{\sigma}})}{\partial \phi'} = \frac{\partial \bar{\sigma}(\widehat{\boldsymbol{\sigma}})}{\partial \phi''} = \frac{\bar{\sigma}^{1-m}}{2m}, \tag{A.12}$$

$$\left[\frac{\partial \phi'}{\partial \mathbf{s}'}\right] = \left[m\left\{ \left(\widetilde{S}_I' - \widetilde{S}_{II}'\right)\left|\widetilde{S}_I' - \widetilde{S}_{II}'\right|^{m-2}\right\} - m\left\{\left(\widetilde{S}_I' - \widetilde{S}_{II}'\right)\left|\widetilde{S}_I' - \widetilde{S}_{II}'\right|^{m-2}\right\} \right], \left[\frac{\partial \phi'}{\partial \mathbf{s}''}\right]$$

$$= \begin{bmatrix} m\left\{ \left(2\widetilde{S}_{II}'' + \widetilde{S}_I''\right)\left|2\widetilde{S}_{II}'' + \widetilde{S}_I''\right|^{m-2} + 2\left(2\widetilde{S}_I'' + \widetilde{S}_{II}''\right)\left|2\widetilde{S}_I'' + \widetilde{S}_{II}''\right|^{m-2}\right\} \\ m\left\{ 2\left(2\widetilde{S}_{II}'' + \widetilde{S}_I''\right)\left|2\widetilde{S}_{II}'' + \widetilde{S}_I''\right|^{m-2} + \left(2\widetilde{S}_I'' + \widetilde{S}_{II}''\right)\left|2\widetilde{S}_I'' + \widetilde{S}_{II}''\right|^{m-2}\right\} \end{bmatrix}^T,$$

$$\tag{A.13}$$

$$\left[\frac{\partial \widetilde{\mathbf{s}}'}{\partial \mathbf{s}'}\right] = \begin{bmatrix} \frac{1}{2} + \frac{(S_{xx}' - S_{yy}')}{2\sqrt{\Delta'}} & \frac{1}{2} - \frac{(S_{xx}' - S_{yy}')}{2\sqrt{\Delta'}} & \frac{2S_{xy}'}{\sqrt{\Delta'}} \\ \frac{1}{2} - \frac{(S_{xx}' - S_{yy}')}{2\sqrt{\Delta'}} & \frac{1}{2} + \frac{(S_{xx}' - S_{yy}')}{2\sqrt{\Delta'}} & -\frac{2S_{xy}'}{\sqrt{\Delta'}} \end{bmatrix},$$

$$\left[\frac{\partial \widetilde{\mathbf{s}}''}{\partial \mathbf{s}''}\right] = \begin{bmatrix} \frac{1}{2} + \frac{(S_{xx}'' - S_{yy}'')}{2\sqrt{\Delta''}} & \frac{1}{2} - \frac{(S_{xx}'' - S_{yy}'')}{2\sqrt{\Delta''}} & \frac{2S_{xy}''}{\sqrt{\Delta''}} \\ \frac{1}{2} - \frac{(S_{xx}'' - S_{yy}'')}{2\sqrt{\Delta''}} & \frac{1}{2} + \frac{(S_{xx}'' - S_{yy}'')}{2\sqrt{\Delta''}} & -\frac{2S_{xy}''}{\sqrt{\Delta''}} \end{bmatrix}, \tag{A.14}$$

where

$$\Delta' = \left(S_{xx}' - S_{yy}'\right)^2 + 4S_{xy}',$$
$$\Delta'' = \left(S_{xx}'' - S_{yy}''\right)^2 + 4S_{xy}''. \tag{A.15}$$

And,

$$\left[\frac{\partial \mathbf{s}'}{\partial \bar{\boldsymbol{\sigma}}}\right] = [\mathbf{L}'] = \begin{bmatrix} L_{11}' & L_{12}' & 0 \\ L_{21}' & L_{22}' & 0 \\ 0 & 0 & L_{66}' \end{bmatrix},$$

$$\left[\frac{\partial \mathbf{s}''}{\partial \bar{\boldsymbol{\sigma}}}\right] = [\mathbf{L}''] = \begin{bmatrix} L_{11}'' & L_{12}'' & 0 \\ L_{21}'' & L_{22}'' & 0 \\ 0 & 0 & L_{66}'' \end{bmatrix}, \tag{A.16}$$

$$\left[\frac{\partial \widehat{\boldsymbol{\sigma}}}{\partial \boldsymbol{\sigma}}\right] = \begin{bmatrix} \cos^2\theta & \sin^2\theta & -2\cos\theta\sin\theta \\ \sin^2\theta & \cos^2\theta & 2\cos\theta\sin\theta \\ \cos\theta\sin\theta & -\cos\theta\sin\theta & \cos^2\theta - \sin^2\theta \end{bmatrix}. \tag{A.17}$$
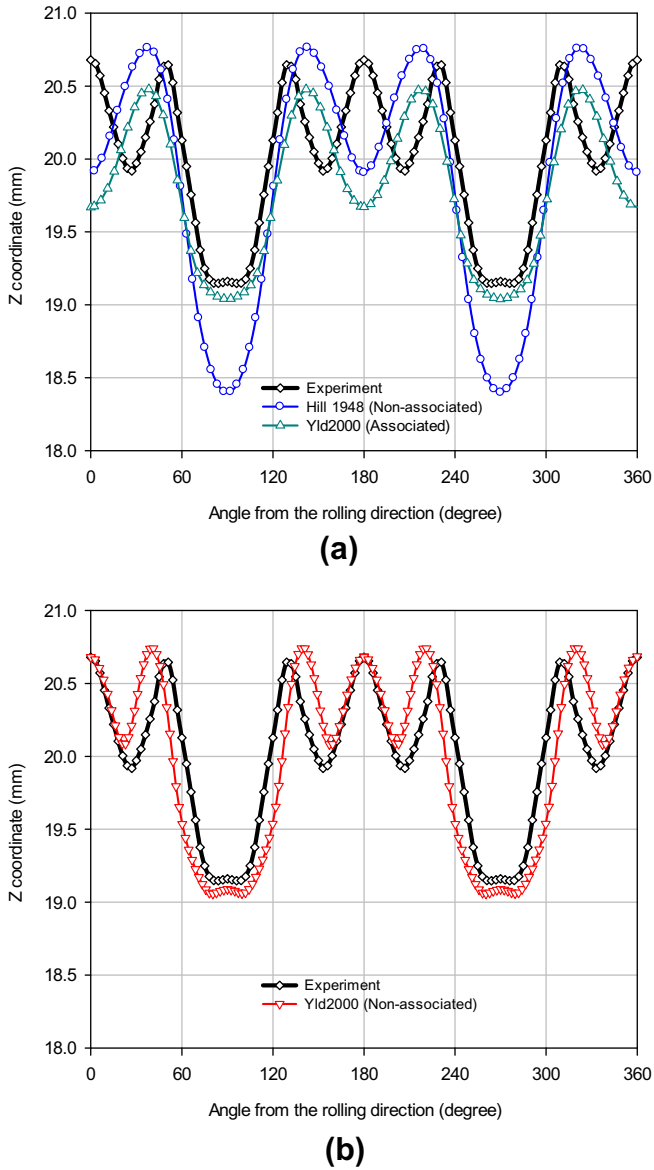
(a)

(b)

Fig. 9. Comparison of measured and calculated earing profiles of AA5042: (a) based on the non-associated model with Hill48 and the associated model with Yld2000, (b) based on the non-associated model with Yld2000.
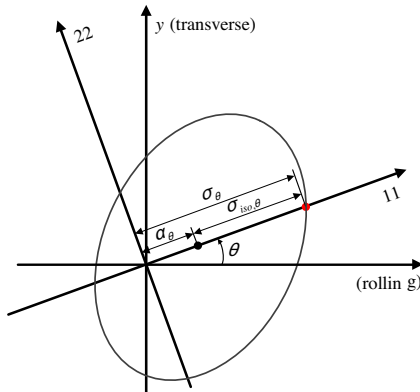

Fig. B.1. Schematic view of the reference coordinate system aligned along the rolling direction and the rotated coordinate system aligned along the simple tension (θ) direction.

As for the derivatives, $\frac{\partial \bar{\sigma}(\boldsymbol{\sigma})}{\partial \alpha_k}$, the following chain rules can be applied neglecting the high order variations for simplicity,

$$\frac{\partial \bar{\sigma}(\boldsymbol{\sigma})}{\partial \alpha_k} = \frac{\partial \bar{\sigma}(\boldsymbol{\sigma})}{\partial \phi'} \frac{\partial \phi'}{\partial \tilde{\mathbf{s}}'} \frac{\partial \tilde{\mathbf{s}}'}{\partial \mathbf{s}'} \frac{\partial \mathbf{s}'}{\partial \alpha_k} \quad (k = 1, 2, 7),$$

$$\frac{\partial \bar{\sigma}(\boldsymbol{\sigma})}{\partial \alpha_k} = \frac{\partial \bar{\sigma}(\boldsymbol{\sigma})}{\partial \phi''} \frac{\partial \phi''}{\partial \tilde{\mathbf{s}}''} \frac{\partial \tilde{\mathbf{s}}''}{\partial \mathbf{s}''} \frac{\partial \mathbf{s}''}{\partial \alpha_k} \quad (k = 3, 4, 5, 6, 8),$$

$$(A.18)$$

where

$$\left[\frac{\partial \mathbf{s}'}{\partial \alpha_1}\right] = \begin{bmatrix} 2/3 & -1/3 & 0 \\ 0 & 0 & 0 \\ 0 & 0 & 0 \end{bmatrix} \widehat{\boldsymbol{\sigma}}, \quad \left[\frac{\partial \mathbf{s}'}{\partial \alpha_2}\right] = \begin{bmatrix} 0 & 0 & 0 \\ -1/3 & 2/3 & 0 \\ 0 & 0 & 0 \end{bmatrix} \widehat{\boldsymbol{\sigma}},$$

$$\left[\frac{\partial \mathbf{s}''}{\partial \alpha_3}\right] = \frac{1}{9} \begin{bmatrix} -2 & 1 & 0 \\ 4 & -2 & 0 \\ 0 & 0 & 1 \end{bmatrix} \widehat{\boldsymbol{\sigma}}, \quad \left[\frac{\partial \mathbf{s}''}{\partial \alpha_4}\right] = \frac{1}{9} \begin{bmatrix} 2 & -4 & 0 \\ -4 & 8 & 0 \\ 0 & 0 & 1 \end{bmatrix} \widehat{\boldsymbol{\sigma}},$$

$$(A.19)$$

$$\left[\frac{\partial \mathbf{s}''}{\partial \alpha_5}\right] = \frac{1}{9} \begin{bmatrix} 8 & -4 & 0 \\ -4 & 2 & 0 \\ 0 & 0 & 0 \end{bmatrix} \widehat{\boldsymbol{\sigma}}, \quad \left[\frac{\partial \mathbf{s}''}{\partial \alpha_6}\right] = \frac{1}{9} \begin{bmatrix} -2 & 4 & 0 \\ 1 & -2 & 0 \\ 0 & 0 & 0 \end{bmatrix} \widehat{\boldsymbol{\sigma}},$$

$$\left[\frac{\partial \mathbf{s}'}{\partial \alpha_7}\right] = \left[\frac{\partial \mathbf{s}''}{\partial \alpha_8}\right] = \begin{bmatrix} 0 & 0 & 0 \\ 0 & 0 & 0 \\ 0 & 0 & 1 \end{bmatrix} \widehat{\boldsymbol{\sigma}}.$$

As for the derivatives, $\frac{\partial \left(\frac{\partial \bar{\sigma}(\boldsymbol{\sigma})}{\partial \boldsymbol{\sigma}}\right)}{\partial \alpha_k}$, the following chain rules can be applied,

$$\frac{\partial \left(\frac{\partial \bar{\sigma}(\boldsymbol{\sigma})}{\partial \boldsymbol{\sigma}}\right)}{\partial \alpha_k} = \frac{\partial \bar{\sigma}(\boldsymbol{\sigma})}{\partial \phi'} \frac{\partial \left(\frac{\partial \phi'}{\partial \tilde{\mathbf{s}}'}\right)}{\partial \alpha_k} \frac{\partial \tilde{\mathbf{s}}'}{\partial \mathbf{s}'} \frac{\partial \mathbf{s}'}{\partial \widehat{\boldsymbol{\sigma}}} \frac{\partial \widehat{\boldsymbol{\sigma}}}{\partial \boldsymbol{\sigma}} + \frac{\partial \bar{\sigma}(\boldsymbol{\sigma})}{\partial \phi'} \frac{\partial \phi'}{\partial \tilde{\mathbf{s}}'} \frac{\partial \left(\frac{\partial \tilde{\mathbf{s}}'}{\partial \widehat{\boldsymbol{\sigma}}}\right)}{\partial \alpha_k} \frac{\partial \mathbf{s}'}{\partial \widehat{\boldsymbol{\sigma}}} \frac{\partial \widehat{\boldsymbol{\sigma}}}{\partial \boldsymbol{\sigma}}$$

$$+ \frac{\partial \bar{\sigma}(\boldsymbol{\sigma})}{\partial \phi'} \frac{\partial \phi'}{\partial \tilde{\mathbf{s}}'} \frac{\partial \tilde{\mathbf{s}}'}{\partial \mathbf{s}'} \frac{\partial \left(\frac{\partial \mathbf{s}'}{\partial \widehat{\boldsymbol{\sigma}}}\right)}{\partial \alpha_k} \frac{\partial \widehat{\boldsymbol{\sigma}}}{\partial \boldsymbol{\sigma}} \quad (k = 1, 2, 7),$$

$$\frac{\partial \left(\frac{\partial \bar{\sigma}(\boldsymbol{\sigma})}{\partial \boldsymbol{\sigma}}\right)}{\partial \alpha_k} = \frac{\partial \bar{\sigma}(\boldsymbol{\sigma})}{\partial \phi''} \frac{\partial \left(\frac{\partial \phi''}{\partial \tilde{\mathbf{s}}''}\right)}{\partial \alpha_k} \frac{\partial \tilde{\mathbf{s}}''}{\partial \mathbf{s}''} \frac{\partial \mathbf{s}''}{\partial \widehat{\boldsymbol{\sigma}}} \frac{\partial \widehat{\boldsymbol{\sigma}}}{\partial \boldsymbol{\sigma}} + \frac{\partial \bar{\sigma}(\boldsymbol{\sigma})}{\partial \phi''} \frac{\partial \phi''}{\partial \tilde{\mathbf{s}}''} \frac{\partial \left(\frac{\partial \tilde{\mathbf{s}}''}{\partial \widehat{\boldsymbol{\sigma}}}\right)}{\partial \alpha_k} \frac{\partial \mathbf{s}''}{\partial \widehat{\boldsymbol{\sigma}}} \frac{\partial \widehat{\boldsymbol{\sigma}}}{\partial \boldsymbol{\sigma}}$$

$$(A.20)$$

$$+ \frac{\partial \bar{\sigma}(\boldsymbol{\sigma})}{\partial \phi''} \frac{\partial \phi''}{\partial \tilde{\mathbf{s}}''} \frac{\partial \tilde{\mathbf{s}}''}{\partial \mathbf{s}''} \frac{\partial \left(\frac{\partial \mathbf{s}''}{\partial \widehat{\boldsymbol{\sigma}}}\right)}{\partial \alpha_k} \frac{\partial \widehat{\boldsymbol{\sigma}}}{\partial \boldsymbol{\sigma}} \quad (k = 3, 4, 5, 6, 8),$$

where

$$\frac{\partial \left(\frac{\partial \phi'}{\partial \tilde{\mathbf{s}}'}\right)}{\partial \alpha_k} = \frac{\partial^2 \phi'}{\partial \tilde{\mathbf{s}}' \partial \tilde{\mathbf{s}}'} \frac{\partial \tilde{\mathbf{s}}'}{\partial \mathbf{s}'} \frac{\partial \mathbf{s}'}{\partial \alpha_k} \quad (k = 1, 2, 7),$$

$$\frac{\partial \left(\frac{\partial \phi''}{\partial \tilde{\mathbf{s}}''}\right)}{\partial \alpha_k} = \frac{\partial^2 \phi''}{\partial \tilde{\mathbf{s}}'' \partial \tilde{\mathbf{s}}''} \frac{\partial \tilde{\mathbf{s}}''}{\partial \mathbf{s}''} \frac{\partial \mathbf{s}''}{\partial \alpha_k} \quad (k = 3, 4, 5, 6, 8),$$

$$(A.21)$$

$$\left[\frac{\partial^2 \phi'}{\partial \tilde{\mathbf{s}}' \partial \tilde{\mathbf{s}}'}\right] = m(m-1) \begin{bmatrix} \left(\tilde{S}_I' - S_{II}'\right)^{m-2} & -\left(\tilde{S}_I' - S_{II}'\right)^{m-2} \\ -\left(\tilde{S}_I' - S_{II}'\right)^{m-2} & \left(\tilde{S}_I' - S_{II}'\right)^{m-2} \end{bmatrix},$$

$$\left[\frac{\partial^2 \phi''}{\partial \tilde{\mathbf{s}}'' \partial \tilde{\mathbf{s}}''}\right] = m(m-1) \begin{bmatrix} \left|2\tilde{S}_{II}'' + \tilde{S}_I''\right|^{m-2} + 4\left|2\tilde{S}_I'' + \tilde{S}_{II}''\right|^{m-2} & 2\left|2\tilde{S}_{II}'' + \tilde{S}_I''\right|^{m-2} + 2\left|2\tilde{S}_I'' + \tilde{S}_{II}''\right|^{m-2} \\ 2\left|2\tilde{S}_{II}'' + \tilde{S}_I''\right|^{m-2} + 2\left|2\tilde{S}_I'' + \tilde{S}_{II}''\right|^{m-2} & 4\left|2\tilde{S}_{II}'' + \tilde{S}_I''\right|^{m-2} + \left|2\tilde{S}_I'' + \tilde{S}_{II}''\right|^{m-2} \end{bmatrix},$$

$$(A.22)$$

$$\frac{\partial \left(\frac{\partial \tilde{\mathbf{s}}'}{\partial \mathbf{s}'}\right)}{\partial \alpha_k} = \frac{\partial^2 \tilde{\mathbf{s}}'}{\partial \mathbf{s}' \partial \mathbf{s}'} \frac{\partial \mathbf{s}'}{\partial \alpha_k} \quad (k = 1, 2, 7),$$

$$\frac{\partial \left(\frac{\partial \tilde{\mathbf{s}}''}{\partial \mathbf{s}''}\right)}{\partial \alpha_k} = \frac{\partial^2 \tilde{\mathbf{s}}''}{\partial \mathbf{s}'' \partial \mathbf{s}''} \frac{\partial \mathbf{s}''}{\partial \alpha_k} \quad (k = 3, 4, 5, 6, 8),$$

$$(A.23)$$

$$\left[\frac{\partial^2 \tilde{S}_I'}{\partial \mathbf{s}' \partial \mathbf{s}'}\right] = -\left[\frac{\partial^2 \tilde{S}_{II}'}{\partial \mathbf{s}' \partial \mathbf{s}'}\right] = \begin{bmatrix} \frac{1}{2\sqrt{\Delta'}} - \frac{\left(S_{xx}' - S_{yy}'\right)^2}{2(\Delta')^{3/2}} & -\frac{1}{2\sqrt{\Delta'}} + \frac{\left(S_{xx}' - S_{yy}'\right)^2}{2(\Delta')^{3/2}} & \frac{2\left(S_{yy}' - S_{xx}'\right)S_{xy}'}{(\Delta')^{3/2}} \\ -\frac{1}{2\sqrt{\Delta'}} + \frac{\left(S_{xx}' - S_{yy}'\right)^2}{2(\Delta')^{3/2}} & \frac{1}{2\sqrt{\Delta'}} - \frac{\left(S_{xx}' - S_{yy}'\right)^2}{2(\Delta')^{3/2}} & \frac{2\left(S_{xx}' - S_{yy}'\right)S_{xy}'}{(\Delta')^{3/2}} \\ \frac{2\left(S_{yy}' - S_{xx}'\right)S_{xy}'}{(\Delta')^{3/2}} & \frac{2\left(S_{xx}' - S_{yy}'\right)S_{xy}'}{(\Delta')^{3/2}} & \frac{2}{\sqrt{\Delta'}} - \frac{8S_{xy}'^2}{(\Delta')^{3/2}} \end{bmatrix},$$

$$\left[\frac{\partial^2 \widetilde{S}''_I}{\partial s'' \partial s''}\right] = -\left[\frac{\partial^2 \widetilde{S}''_{II}}{\partial s'' \partial s''}\right] = \begin{bmatrix} \frac{1}{2\sqrt{\Delta''}} - \frac{(S''_{xx}-S''_{yy})^2}{2(\Delta'')^{3/2}} & -\frac{1}{2\sqrt{\Delta''}} + \frac{(S''_{xx}-S''_{yy})^2}{2(\Delta'')^{3/2}} & \frac{2(S''_{yy}-S'_{xx})S'_{xy}}{(\Delta'')^{3/2}} \\ -\frac{1}{2\sqrt{\Delta''}} + \frac{(S''_{xx}-S''_{yy})^2}{2(\Delta'')^{3/2}} & \frac{1}{2\sqrt{\Delta''}} - \frac{(S''_{xx}-S''_{yy})^2}{2(\Delta'')^{3/2}} & \frac{2(S''_{xx}-S''_{yy})S''_{xy}}{(\Delta'')^{3/2}} \\ \frac{2(S''_{yy}-S''_{xx})S''_{xy}}{(\Delta'')^{3/2}} & \frac{2(S''_{xx}-S''_{yy})S''_{xy}}{(\Delta'')^{3/2}} & \frac{2}{\sqrt{\Delta''}} - \frac{8S''^2_{xy}}{(\Delta'')^{3/2}} \end{bmatrix},$$

(A.24)

and

$$\left[\frac{\partial\left(\frac{\partial s'}{\partial \boldsymbol{\sigma}}\right)}{\partial \alpha_k}\right] = \left[\frac{\partial \mathbf{L}'}{\partial \alpha_k}\right] \quad (k = 1, 2, 7),$$

$$\left[\frac{\partial\left(\frac{\partial s''}{\partial \boldsymbol{\sigma}}\right)}{\partial \alpha_k}\right] = \left[\frac{\partial \mathbf{L}''}{\partial \alpha_k}\right] \quad (k = 3, 4, 5, 6, 8),$$

(A.25)

while

$$\begin{bmatrix} \frac{\partial L'_{11}}{\partial \alpha_1} & \frac{\partial L'_{11}}{\partial \alpha_2} & \frac{\partial L'_{11}}{\partial \alpha_7} \\ \frac{\partial L'_{12}}{\partial \alpha_1} & \frac{\partial L'_{12}}{\partial \alpha_2} & \frac{\partial L'_{12}}{\partial \alpha_7} \\ \frac{\partial L'_{23}}{\partial \alpha_1} & \frac{\partial L'_{21}}{\partial \alpha_2} & \frac{\partial L'_{21}}{\partial \alpha_7} \\ \frac{\partial L'_{22}}{\partial \alpha_1} & \frac{\partial L'_{22}}{\partial \alpha_2} & \frac{\partial L'_{22}}{\partial \alpha_7} \\ \frac{\partial L'_{66}}{\partial \alpha_1} & \frac{\partial L'_{66}}{\partial \alpha_2} & \frac{\partial L'_{66}}{\partial \alpha_7} \end{bmatrix} = \begin{bmatrix} 2/3 & 0 & 0 \\ -1/3 & 0 & 0 \\ 0 & -1/3 & 0 \\ 0 & 2/3 & 0 \\ 0 & 0 & 1 \end{bmatrix},$$

(A.26)

$$\begin{bmatrix} \frac{\partial L''_{11}}{\partial \alpha_3} & \frac{\partial L''_{11}}{\partial \alpha_4} & \frac{\partial L''_{11}}{\partial \alpha_5} & \frac{\partial L''_{11}}{\partial \alpha_6} & \frac{\partial L''_{11}}{\partial \alpha_8} \\ \frac{\partial L''_{12}}{\partial \alpha_3} & \frac{\partial L''_{12}}{\partial \alpha_4} & \frac{\partial L''_{12}}{\partial \alpha_5} & \frac{\partial L''_{12}}{\partial \alpha_6} & \frac{\partial L''_{12}}{\partial \alpha_8} \\ \frac{\partial L''_{21}}{\partial \alpha_3} & \frac{\partial L''_{21}}{\partial \alpha_4} & \frac{\partial L''_{21}}{\partial \alpha_5} & \frac{\partial L''_{21}}{\partial \alpha_6} & \frac{\partial L''_{21}}{\partial \alpha_8} \\ \frac{\partial L''_{22}}{\partial \alpha_3} & \frac{\partial L''_{22}}{\partial \alpha_4} & \frac{\partial L''_{22}}{\partial \alpha_5} & \frac{\partial L''_{22}}{\partial \alpha_6} & \frac{\partial L''_{22}}{\partial \alpha_8} \\ \frac{\partial L''_{66}}{\partial \alpha_3} & \frac{\partial L''_{66}}{\partial \alpha_4} & \frac{\partial L''_{66}}{\partial \alpha_5} & \frac{\partial L''_{66}}{\partial \alpha_6} & \frac{\partial L''_{66}}{\partial \alpha_8} \end{bmatrix} = \frac{1}{9}\begin{bmatrix} -2 & 2 & 8 & -2 & 0 \\ 1 & -4 & -4 & 4 & 0 \\ 4 & -4 & -4 & 1 & 0 \\ -2 & 8 & 2 & -2 & 0 \\ 0 & 0 & 0 & 0 & 9 \end{bmatrix}.$$

(A.27)

References

Banabic, D., Aretz, H., Comsa, D.S., Paraianu, L., 2005. An improved analytical description of orthotropy in metallic sheets. Int. J. Plast. 21, 493–512.

Barlat, F., Chung, K.S., 1993. Anisotropic Potentials for Plastically Deforming Metals. Model Simul. Mater. Sci. 1, 403–416.

Barlat, F., Lege, D.J., Brem, J.C., 1991. A 6-Component Yield Function for Anisotropic Materials. Int. J. Plast. 7, 693–712.

Barlat, F., Chung, K., Richmond, O., 1993. Strain Rate Potential for Metals and Its Application to Minimum Plastic Work Path Calculations. Int. J. Plast. 9, 51–63.

Barlat, F., Becker, R.C., Hayashida, Y., Maeda, Y., Yanagawa, M., Chung, K., Brem, J.C., Lege, D.J., Matsui, K., Murtha, S.J., Hattori, S., 1997. Yielding description for solution strengthened aluminum alloys. Int. J. Plast. 13, 385–401.

Barlat, F., Brem, J.C., Yoon, J.W., Chung, K., Dick, R.E., Lege, D.J., Pourgoghrat, F., Choi, S.H., Chu, E., 2003. Plane stress yield function for aluminum alloy sheets- part 1: theory. Int. J. Plast. 19, 1297–1319.

Barlat, F., Aretz, H., Yoon, J.W., Karabin, M.E., Brem, J.C., Dick, R.E., 2005. Linear transfomation-based anisotropic yield functions. Int. J. Plast. 21, 1009–1039.

Brunig, M., 1999. Numerical simulation of the large elastic-plastic deformation behavior of hydrostatic stress-sensitive solids. Int. J. Plast. 15, 1237–1264.

Brunig, M., Berger, S., Obrecht, H., 2000. Numerical simulation of the localization behavior of hydrostatic-stress-sensitive metals. Int. J. Mech. Sci. 42, 2147–2166.

Cazacu, O., Plunkett, B., Barlat, F., 2006. Orthotropic yield criterion for hexagonal closed packed metals. Int. J. Plast. 22, 1171–1194.

Chaboche, J.L., 1986. Time-Independent Constitutive Theories for Cyclic Plasticity. Int. J. Plast. 2, 149–188.

Chaboche, J.L., 1991. On Some Modifications of Kinematic Hardening to Improve the Description of Ratchetting Effects. Int. J. Plast. 7, 661–678.

Chung, K., 1984. The analysis of anisotropic hardening in finite-deformation plasticity. Department of Mechanical Engineering, Stanford University, CA.

Chung, K., Richmond, O., 1993. A Deformation-Theory of Plasticity Based on Minimum Work Paths. Int. J. Plast. 9, 907–920.

Chung, K., Lee, S.Y., Barlat, F., Keum, Y.T., Park, J.M., 1996. Finite element simulation of sheet forming based on a planar anisotropic strain-rate potential. Int. J. Plast. 12, 93–115.

Chung, K., Barlat, F., Brem, J.C., Lege, D.J., Richmond, O., 1997. Blank Shape Design for a Planar Anisotropic Sheet Based on Ideal Sheet Forming Design Theory and FEM Analysis. Int. J. Mech. Sci. 39, 105–120.

Chung, K., Lee, M.G., Kim, D., Kim, C., Wenner, M.L., Barlat, F., 2005. Spring-back evaluation of automotive sheets based on isotropic–kinematic hardening laws and non-quadratic anisotropic yield functions, Part I: theory and formulation. Int. J. Plast. 21, 861–882.

Chung, K., Kim, D., Park, T., 2011. Analytical derivation of earing in circular cup drawing based on simple tension properties. Eur. J. Mech. A-Solid 30, 275–280.

Cvitanic, V., Vlak, F., Lozina, Z., 2008. A finite element formulation based on non-associated plasticity for sheet metal forming. Int. J. Plast. 24, 646–687.

Drucker, D.C., 1959. A Definition of Stable Inelastic Material. ASME, J. Appl. Mech. 26, 101–106.

Hill, R., 1948. A Theory of the Yielding and Plastic Flow of Anisotropic Metals. Proc. R. Soc. Lon. Ser.-A 193, 281–297.

Hill, R., 1979. Theoretical Plasticity of Textured Aggregates. Math. Proc. Cambridge 85, 179–191.

Hill, R., 1987. Constitutive Dual Potentials in Classical Plasticity. J. Mech. Phys. Solids 35, 23–33.

Karafillis, A.P., Boyce, M.C., 1993. A General Anisotropic Yield Criterion Using Bounds and a Transformation Weighting Tensor. J. Mech. Phys. Solids 41, 1859–1886.

Kim, D., Barlat, F., Bouvier, S., Rabahallah, M., Balan, T., Chung, K., 2007. Non-quadratic anisotropic potentials based on linear transformation of plastic strain rate. Int. J. Plast. 23, 1380–1399.

Lademo, O.G., Hopperstad, O.S., Langseth, M., 1999. An evaluation of yield criteria and flow rules for aluminium alloys. Int. J. Plast. 15, 191–208.

Mohr, D., Dunand, M., Kim, K.H., 2010. Evaluation of associated and non-associated quadratic plasticity models for advanced high strength steel sheets under multi-axial loading. Int. J. Plast. 26, 939–956.

Simo, J.C., Hughes, T.J.R., 1998. Computational inelasticity. In: Interdisciplinary Applied Mathematics. Springer-Verlag, Berlin.

Soare, S.C., Barlat, F., 2011. A study of the Yld2004 yield function and one extension in polynomial form: A new implementation algorithm, modeling range, and earing predictions for aluminum alloy sheets. Eur. J. Mech. A-Solid 30, 807–819.

Spitzig, W.A., Sober, R.J., Richmond, O., 1975. Pressure-Dependence of Yielding and Associated Volume Expansion in Tempered Martensite. Acta Metal. 23, 885–893.

Stoughton, T.B., 2002. A non-associated flow rule for sheet metal forming. Int. J. Plast. 18, 687–714.

Stoughton, T.B., Yoon, J.W., 2004. A pressure-sensitive yield criterion under a non-associated flow rule for sheet metal forming. Int. J. Plast. 20, 705–731.

Stoughton, T.B., Yoon, J.W., 2006. Review of Drucker's postulate and the issue of plastic stability in metal forming, Int. J. Plast. 22, 391–433.

Stoughton, T.B., Yoon, J.W., 2008. On the existence of indeterminate solutions to the equations of motion under non-associated flow, Int. J. Plast. 24, 583–613.

Taherizadeh, A., Green, D.E., Ghaei, A., Yoon, J.W., 2010. A non-associated constitutive model with mixed iso-kinematic hardening for finite element simulation of sheet metal forming. Int. J. Plast. 26, 288–309.

Taherizadeh, A., Green, D.E., Yoon, J.W., 2011. Evaluation of advanced anisotropic models with mixed hardening for general associated and non-associated flow metal plasticity. Int. J. Plast. 27, 1781–1802.

Yoon, J.W., Dick, R.E., 2011. BM1-earing evolution during drawing and ironing processes. In: Huh, H., Chung, K., Han, S.S., Chung, W.J. (Ed.), The NUMISHEET 2011 Benchmark Study of the 8th International Conference and Workshop on Numerical Simulation of 3D Sheet Metal Forming Processes, Korea.

Yoon, J.W., Barlat, F., Chung, K., Pourboghrat, F., Yang, D.Y., 2000. Earing predictions based on asymmetric nonquadratic yield function. Int. J. Plast. 16, 1075–1104.

Yoon, J.W., Barlat, F., Dick, R.E., Chung, K., Kang, T.J., 2004. Plane stress yield function for aluminum alloy sheets-part II: FE formulation and its implementation. Int. J. Plast. 20, 495–522.

Yoon, J.W., Barlat, F., Dick, R.E., Karabin, M.E., 2006. Prediction of six or eight ears in a drawn cup based on a new anisotropic yield function. Int. J. Plast. 22, 174–193.

Yoon, J.H., Cazacu, O., Yoon, J.W., Dick, R.E., 2010. Earing predictions for strongly textured aluminum sheets. Int. J. Mech. Sci. 52, 1563–1578.

Yoon, J.W., Dick, R.E., Barlat, F., 2011. A new analytical theory for earing generated from anisotropic plasticity. Int. J. Plast. 27, 1165–1184.